

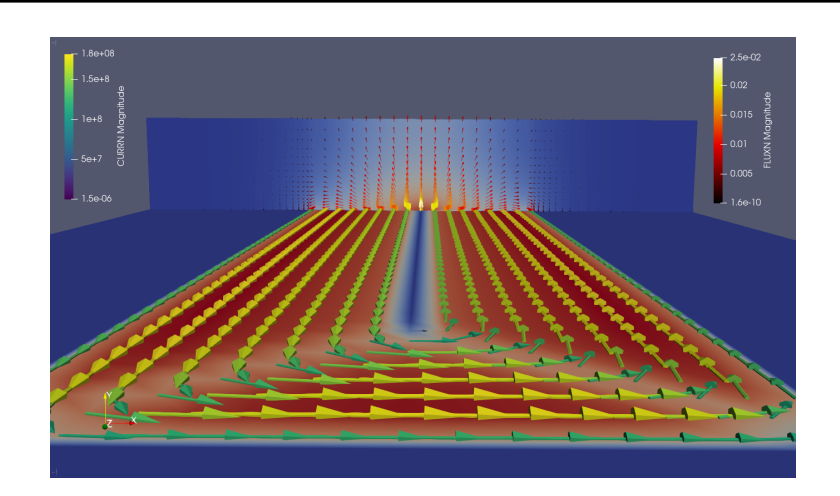


MASTER THESIS

MSc of Modelling for Science and Engineering

Experimental validation of a new HPC modelling tool for High Temperature Superconductivity

Oriol Fernández Serracanta



Directors:

José Lorenzo (Barcelona Supercomputing Center) Mervi Mantsinen (ICREA and Barcelona Supercomputing Center)

Year 2021

| To all the people who encouraged, helped and lived with me this adventure. |
|--|
| |
| |
| |
| |
| |
| |
| |
| |
| |
| |
| |
| |
| |

Acknowledgements

I would like to give a special thank to my supervisors José Lorenzo and Mervi Mantsinen, who guided and helped me in a very enthusiastic way in these worlds of Superconductivity and Modelling. First during the internship at the Barcelona Supercomputing Center where they were advising and accompanying me in all the issues I had in a very attentive and close way. And afterwards on the thesis guiding me with all the topics, being very responsive and involved with the supervision, and giving lots of advice for both the written and the dissertation part. I could not have better supervisors for both the internship and the thesis.

Moreover, I would like to thank Xavier Granados and Neil Lamas from ICMAB-CSIC (Institute of Materials Science of Barcelona) for the experimental data given for the simulations as well as the discussions about the experiments.

I would like to thank my girlfriend Mar and my parents who, despite not being familiarised at all with the topic helped me with all they could regarding the structure of the thesis, English language and formatting issues as well as giving me support during all this time. Thanks to all my master colleagues, Josep, Jota, and Sandra, who joined and lived with me this strange year and helped me to overcome this course in the best possible way. Also, I would like to thank my friends and university colleagues who despite being further from these topics were always by my side giving me good times and moments of disconnection, even if I were fully busy and focused on the master or if we were confined.

In addition, I thank Alba for giving me a hand on these last days by helping me on polishing the most relevant parts of the Thesis as well as giving me support on these final moments.

Finally, I would like to express my special thanks to my sister Maria and Adrià who, again like with the Bachelor Thesis, found moments for helping me with the thesis, discussing topics of this work, and spending their time on reviewing and giving advice on this thesis, despite being very busy with their university and every-day obligations.

Oriol Fernández Serracanta

Abstract

Superconductivity is a physical phenomenon of some materials that allow them to conduct electrical current without resistance. This property has many applications which are currently under development due to its complicated features. In particular, some Type-II High Temperature Superconductors are promising for building strong electromagnets or carrying large amounts of current in extreme conditions like those at CERN, ITER and possible future fusion reactors. However, both its attainment and related experiments are highly expensive and difficult to control. Predicting accurately and efficiently the magnetic response of High Temperature Superconductors is of high importance in numerous applications such as energy transport and storage, trapped-field magnets, or magnetic shielding.

Here, we present a novel contribution to achieve a multiphysics tool able to simulate accurately High Temperature Superconductors (HTS). Our method consists overall in simulating an HTS tape with magnet, which is a module of the HPC code *Alya* developed in the BSC (Barcelona Supercomputing Center). A detailed description of the module and the setup of the simulations is provided in this work. Furthermore, these simulations are validated with experimental data provided by ICMAB (Institute of Materials Science of Barcelona).

Our results indicate that magnet could be used for two-dimensional and three-dimensional simulations of an HTS tape, both with a good agreement with the experimental data. However, it was not able to reproduce minor asymmetries in the vertical magnetic field component observed in the experiments. New implementations have been added in the code in order to introduce a magnetic field dependent Critical Current on the superconducting tape. Finally, a quantitative study showed that the 3D simulation achieved slightly better results than the 2D cases. Overall, there are no fundamentally different results between the simulations while all of them showed good agreement with experimental data.

Our results demonstrate how Alya and its magnet module can simulate accurately an HTS experiment. With further validations and upgrades, it is expected to become a useful multiphysics tool to simulate complex superconductivity cases. For example, it could help us to improve our understanding of the properties of superconducting materials through simulations. With simulations, we may also be able to identify non-feasible experiments (e.g. due to *Quench* phenomena) before carrying them out, thus saving a lot of time and effort. We anticipate that this thesis is a starting point for using Alya multiphysics code to help and progress further in the field of Superconductivity, more concretely the HTS topic.

Resum

La Superconductivitat és un fenomen físic d'alguns materials que els permet conduir electricitat sense resistència. Aquesta propietat té moltes aplicacions encara en desenvolupament a causa de les seves complexes característiques. Concretament alguns superconductors d'Alta Temperatura de tipus-II tenen potencial per construir electroimants molt potents o per transportar grans quantitats de corrent en condicions extremes com els del CERN, ITER i possibles reactors de fusió. Tot i així, tant la seva obtenció com els experiments que es duen a terme són d'un gran cost econòmic i difícils de controlar. Predir amb precisió i eficiència la resposta magnètica d'aquests superconductors és de gran importància en diverses aplicacions com en el transport o emmagatzematge d'energia, imants que atrapen el camp o escuts magnètics.

En aquest treball es presenta una contribució per assolir un codi de multifísica capaç de simular amb precisió Superconductors d'Alta Temperatura (HTS). El mètode emprat consisteix en simular una cinta HTS amb el mòdul magnet, mòdul del codi HPC Alya desenvolupat al BSC(Barcelona Supercomputing Center). També es farà una descripció detallada del mòdul. Posteriorment aquestes simulacions seran validades amb dades experimentals de l'ICMAB (Institut de Ciències de Materials de Barcelona).

Els resultats obtinguts indiquen que el mòdul reprodueix amb precisió experiments 2D i 3D de la cinta HTS. Tot i així, no és capaç de reproduir asimetries menors en el camp magnètic vertical observades en experiments. Noves implementacions s'han afegit al codi per poder introduir un Corrent Crític dependent del camp magnètic a la cinta superconductora. Finalment, l'anàlisi quantitatiu mostra que les simulacions 3D presenten uns resultats lleugerament més precisos que els altres casos, tot i així no hi ha diferències substancials entre les diferents simulacions.

Els nostres resultats mostren com Alya i el seu mòdul magnet permet simular de forma fiable un experiment amb HTS. Amb posteriors validacions i millores s'espera que el codi pugui esdevenir una eina de multifísica capaç de simular problemes de superconductivitat complexos. Per exemple, serà possible entendre les propietats d'alguns materials a través de les simulacions o obtenir resultats d'experiments impossibles al laboratori, com per exemple buscar les condicions sota les quals es pot trobar el fenomen de Quench en superconductors. Presentem aquest treball com a punt de partida per fer servir el codi Alya per tal d'ajudar a progressar en el camp de la Superconductivitat, més concretament en el de Superconductors d'Alta Temperatura.

List of Figures

| 2.1 2.2 2.3 | Scheme of conductivities of many materials from Solazzo et al. [2019] Example of Critical Surface by Lorenzo [2019] | 10 13 |
|-------------------|---|----------|
| 3.1 | General Workflow of the Alya system from CASE department [2021] | 26 |
| 4.1 4.2 | Mapping of B_z measurements from ICMAB (courtesy of Neil Lamas, ICMAB) Scheme of the THEVA tape (obtained from THEVA [accessed: February 9, 2022]) | 36 |
| 4.3 4.4 | 2022]) | 37 38 |
| 4.5 | generated by the superconductor tape (T) | 39 39 |
| 4.6 4.7 | B_y field at $400\mu m$ of the tape for the small 2D domain, the tape goes from $-0.006 - 0.006$ m according to the tape width of 12 mm | 40 |
| 4.8 | (a) Plot of the Z component of the Current and (b) Magnetic field generated by the superconductor tape for the Increased Air Domain experiment | 43 |
| 4.9 | Comparison for B_y at $400\mu m$ of the case of the small domain and the new case of the large domain without Self-Field | 44 |
| 4.10 | Current in terms of the magnetic field intensity $ B $ | 44 |
| | B_y profile at 400 μm for the case with $J_c(\theta, \mathbf{B})$ | 46 |
| 4.13 | has its peaks | 47 |
| 4.14 | (b) at 10 μm , (c) at 20 μm and in (d) at 40 μm | 48 |
| 4.15 | Comparison of B_y at $400\mu m$ for different lengths of tapes and experimental values | 50 |
| 4.16 | 3D plot of the superconducting tape, the vectors show the current flowing in the tape | 51 |

| 4.17 | Current and Magnetic field of the new 3D simulation | 52 |
|------|--|----|
| 4.18 | B_y at $400\mu m$ for the 3D case with $J_c(\theta, \mathbf{B})$ | 52 |
| 4.19 | Final comparison for Magnetic Field profiles | 53 |

Contents

| \mathbf{A} | Abstract | | iii |
|--------------|-----------------|--|-----|
| Li | List of Figures | | |
| 1 | Intr | roduction | 1 |
| | 1.1 | Objectives | 2 |
| | 1.2 | Methodology | 3 |
| | 1.3 | Structure of the thesis | 3 |
| 2 | Phy | sics of Superconductivity | 5 |
| | 2.1 | Maxwell Equations in vacuum | 6 |
| | | 2.1.1 Electromagnetism and Maxwell equations in media | 6 |
| | | 2.1.2 Contour Conditions for the Electromagnetic Field | 8 |
| | 2.2 | Introduction to Superconductivity | 9 |
| | | 2.2.1 Magnetic Shielding | 10 |
| | 2.3 | Superconductor classification | 12 |
| | | 2.3.1 Critical Magnetic Field Criterion | 12 |
| | | 2.3.2 Critical Temperature Criterion | 14 |
| | 2.4 | Applications for Superconductors | 15 |
| | | 2.4.1 Quench in superconductor tapes | 16 |
| | 2.5 | Superconductor Modelling | 16 |
| | | 2.5.1 Modelling the Resistivity | 19 |
| | | 2.5.2 Biot-Savart Law for the Self Field Option | 20 |
| 3 | The | Finite Element Method Alya Code | 21 |
| | 3.1 | The Finite Element Method | 21 |
| | | 3.1.1 Technical Overview of FEM | 22 |
| | 3.2 | Overview of Alya Code | 24 |
| | 3.3 | Main Structure of Alya | 25 |
| | 3.4 | Magnet module | 27 |
| | | 3.4.1 Magnet input files | 27 |
| | | 3.4.2 Other files | 32 |
| | 3.5 | Simulation Guidelines | 33 |
| | | 3.5.1 Problem Preprocessing and Setup | 33 |
| | | 3.5.2 Simulation of the Problem and Model Debugging | 33 |
| | | 3.5.3 Post-processing and Data Visualization | 34 |

| 4 | Res | ults | 3 5 |
|--------------|--------|--|------------|
| | 4.1 | Modelling ICMAB experiment | 35 |
| | | 4.1.1 Considerations for the modelling | 36 |
| | 4.2 | 2D Simulations | 37 |
| | | 4.2.1 2D simulation with Self-Field | 38 |
| | | | 10 |
| | | 4.2.3 Increased Air Domain | 12 |
| | | 4.2.4 Dependence on Magnetic Field Orientation | 13 |
| | | 4.2.5 Results with Angular Dependence | 15 |
| | 4.3 | 3D Simulations for the Tape problem | 19 |
| | | 4.3.1 Tape Length Optimization | 19 |
| | | 4.3.2 3D case with variable Critical Current | 51 |
| | 4.4 | Final Summary and Comparison | 53 |
| 5 | Con | clusions 5 | 55 |
| | 5.1 | | 55 |
| | 5.2 | | 57 |
| | | | 57 |
| | | 1 5 5 | 58 |
| Re | eferei | nces 6 | 3 2 |
| Aı | opene | dix | 3 |
| \mathbf{A} | in tl | | 3 |
| | | | 53 54 |

Chapter 1

Introduction

From all the phenomena in Electromagnetism, Superconductivity rises as one of the most exotic and promising topics. The levitating materials on a railway of magnets when pouring liquid nitrogen or the ability to conduct extremely large amounts of current without losses can attract the attention of many people. However as any topic that outstands in some aspects, it has some drawbacks that must be considered.

Superconductors require very concrete conditions, such as very low temperatures or currents and magnetic fields below a threshold. The lack of any of these conditions leads to the disappearance of the superconductor state and thereupon, fatal consequences for the material. This together with the high cost of obtaining these materials and the fact that they need constant cooling has been a handicap to its commercial use beyond the scientific world.

Out of these fascinating materials, a new type of them has emerged, High-Temperature Superconductors. This type of superconductors has made a big step towards the widespread use of superconductivity. They show superconducting properties at the temperature of liquid Nitrogen (77 K) which is easier and cheaper to obtain than the most used cryogenic coolant, liquid Helium (4 K); and if that was not enough, some of them are part of the Type-II Superconductors, able to resist strong magnetic fields along with high current densities. This compared to the original Superconductors shows a big improvement on properties and usage, from cooling to (4 K) to (77 K) and from resisting external magnetic fields of mT to holding up well fields over 10 or 20 T.

This opens a door to even more applications, such as the possibility to create electromagnets carrying large currents and generating very intense fields. This application can be very helpful for Fusion reactors such as the Tokamak suggested for ITER from ITER project [24 October, 2007] or the further DEMO. The temperatures inside the reactor need to arrive at about 150 million degrees Celsius for the gas in the vacuum to reach the plasma state and hence the fusion reaction occur. These temperatures cannot be held by any material. That is why a technique called magnetic confinement is used, where the ionized gas is kept by an intense magnetic field. This field can be created by high-temperature superconducting tapes because of the intense currents, fields, and forces they will suffer.

In addition, despite having outstanding properties, these materials can still be damaged in many ways, for example, the magnetic fields can generate forces in the material bending it. Another problem can be caused by the big amounts of energy dissipations when strong currents encounter imperfections in the materials (this can lead to a phenomena called *Quench* explained in subsection 2.4.1); and lastly but not less importantly the production cost of these materials is very high.

That is why at BSC an HPC code has been developed in order to simulate this High-Temperature Superconductor behavior, hence we can test and know the limits and properties of these materials by simulating them. In consequence we can also know their properties and how they need to be designed before manufacturing and testing them.

This work aims to explore and start experimental validation of the HPC code Alya for performing accurate simulations of High-Temperature Superconductors. First, we will focus on the study of Electromagnetism applied to the superconducting state, how we can classify the Superconductors and which properties we are expecting to observe on the simulations. Also we will go through the numerical models used to simulate these physical cases, concretely the H-formulation. Afterwards we will explain the main structure of Alya and its modules as well as how these simulations are run in an HPC code using the numerical models explained in the previous chapter. Furthermore a first description of the magnet module will be done with all its input files and how to run simulations for further work.

Finally, we will simulate the experiments carried out by ICMAB with this code. Some physical corrections have been applied to the setup of the simulations in order to achieve similar results to the real data experiments from ICMAB. Later on we will study their capabilities, performance, strengths, and weaknesses by comparing the results obtained with experimental data from ICMAB. Finally, we will suggest future work in order to improve even more this code and reach a multiphysics code able to simulate complex and realistic cases.

1.1 Objectives

The main objective of this MSc thesis is to start the experimental validation of the recently developed magnet module within the Alya system at Barcelona Supercomputing Center with experiments on superconductivity.

The magnet module has been validated with several analytical benchmarks prior to this work. The experimental validation presented in this thesis is a first step towards a multiphysics code able to simulate complex cases involving different physical phenomena. In order to reach this objective, the following tasks are carried out:

- Review the basics of electromagnetism and the theory behind superconductivity with focus on the behavior of Type-II Superconductors. Study the existing formulations of Electromagnetism to model the macroscopic behavior of the superconductors.
- Become familiar with the Finite Element Method and specifically learn how to use Alya, the HPC finite element code developed at Barcelona Supercomputing Center. Investigate and understand the Alya magnet module, and write the first description of its main features and how to use it.

- Understand the features of the tape from the manufacturer THEVA used in the experiment in ICMAB like the crystal tilting, the Current Distribution, and other experimental dependencies.
- Carry out simulations to validate the Alya's magnet module for superconductivity experiments using experimental data from ICMAB

1.2 Methodology

The goal of designing multiphysics software to model superconductors represents a hard problem due to the large amount of physics that must be taken into account and their complexity.

This section discusses the summarized methodology followed in this thesis. Several models have been applied for this thesis to validate the HPC code Alya for experiments on Superconductivity. The following points show the research methodology regarding this thesis.

- 1. Topic Introduction
 - Review literature on Superconductivity and the Physical Problem
 - Researching on HPC codes Alya and familiarization to the HPC environment
- 2. Preprocessing and Setup of the Problem
 - Generation of the Mesh with Gmsh
 - Main Setup of the Problem
- 3. Simulation of the Problem and model Debugging
 - Simulation Launching
 - Output Review and Debugging
- 4. Post-processing and Data Visualization
 - Data Post-processing and Extraction from HPC
 - Visualization of the results with Paraview and extra Post-processing

1.3 Structure of the thesis

The structure of this thesis follows the process undergone by the author when pursuing the tasks presented in Section 1.2.

This Thesis is based on previous research works and studies that cover and focus on all the aspects regarding the Superconductivity topic and the concrete problem. The first part of the thesis is focused on research about Superconductors, concretely the Type-II and their main characteristics together with the modelling of them and the formulations used. Here, we will specifically emphasize on the \boldsymbol{H} formulation. Moreover, research about Alya and its framework were also done. Marenostrum~4 supercomputer has a different operation than regular computers and the HPC Alya demands some time to get used to it and understand its routines, more concretely the ones from the module magnet.

In chapter 2, we will go through the theory on superconductivity and some models to get the basics for doing the simulations. The main Thesis methodology follows the steps mentioned in the above points closely as a guideline for this validation process but in section 3.5, we will go through the steps to follow in order to launch a simulation and visualize results out of it.

The first step was to gain an understanding of the physical problem and Superconductivity. This is summarised in Chapter 2 dedicated mainly to the Physics of Superconductivity. This section is focused on the theoretical basics and some phenomena shown by these materials when they achieve the state of superconductivity. Moreover, a classification has been made in order to differentiate the different types of superconductors. In addition, we go briefly over the main formulations of the Maxwell equations and focus on the \boldsymbol{H} formulation, which is known to be a suitable formulation for the present problem and the one implemented in the Alya magnet module.

In Chapter 3 since Alya uses the Finite Element Method we give a broad description of its basic algorithm. Later on, the particular case of the weak form of the H-Formulation is presented. Afterwards we go through a global summary of the Alya HPC code with its general properties and structure, the main subroutines and all the modules it contains. Furthermore, we explore deeper the magnet module, the one that is validated in this Thesis, and explain all the inputs and options it has, its main structure, and how the simulations are set up.

We present the results obtained from these simulations in Chapter 4. The simulations are presented to show a gradual increase of their complexity starting from 2D simple simulations to 3D simulations including internal dependencies between variables. A summary will be given at the end in order to compare quantitatively all the results obtained and investigate their accuracy by comparing with experimental data.

Finally, in Chapter 5 we expose the conclusions of our work. Also, we discuss the steps that could be followed in order to keep improving this HPC code on simulating more complex problems in the field of Applied Superconductivity. We will also comment on the capabilities of the software and hence the possible improvements on the code itself.

Chapter 2

Physics of Superconductivity

This thesis topic is strongly related to superconductivity, a physical property of some materials based mainly on Electromagnetism principles and Quantum Mechanics effects. Its macroscopic behavior can be numerically reproduced and understood with the use of Electromagnetism principles. Hence, this chapter will focus on summarizing the basics of electromagnetism. Later on, a description of the superconductivity phenomenon will be given together with the classification of the superconductors from the theoretical point of view.

Afterwards some applications and an effect called Quench, which is relevant in superconductivity applications, will be commented on. Finally, some formulations used to simulate Superconductivity will be presented. Among them, special attention is given to the \boldsymbol{H} formulation, which is the one used in Alya (extra information about Alya in CASE department [2021]), the HPC code developed and used at Barcelona Supercomputing Center.

The goal of this chapter is to cover the basics of superconductivity for the reader to understand the phenomena related to Superconductivity as well as the reasons why a multiphysics code is needed for simulating properly this property. Furthermore, the classification is done to give an idea of how the superconductors can be classified and which special properties the simulated Type-II High Temperature Superconducting tape will have. Finally, the summary of the formulations is given to show various ways to describe the electromagnetic behavior of a determined problem. Concretely, the case of the H-Formulation as it is the one used in the module validated in this thesis.

2.1 Maxwell Equations in vacuum

Classical Electromagnetism can be described from many points of view. One possible approach can be the one in López and Costa [2000], which is an inductive method described from the integral forms of the equations. However, the most general way are the Maxwell equations or the differential form described by Maxwell [1865]. In general, in vacuum electromagnetism is governed by these four equations:

$$\nabla \times \boldsymbol{E} = -\frac{\partial \boldsymbol{B}}{\partial t} \tag{2.1.1a}$$

$$\nabla \times \boldsymbol{B} = \mu_0 \cdot \boldsymbol{J} + \mu_0 \epsilon_0 \frac{\partial \boldsymbol{E}}{\partial t}$$
 (2.1.1b)

$$\nabla \cdot \boldsymbol{E} = \frac{\rho}{\epsilon_0} \tag{2.1.1c}$$

$$\nabla \cdot \boldsymbol{B} = 0. \tag{2.1.1d}$$

Here we can see that in any case, as a result of Faraday's law eq. (2.1.1a) and the Ampère's law eq. (2.1.1b), the magnetic and the electric field are coupled when we have a time-dependent electric and magnetic field.

Also, the Gauss law eq. (2.1.1c) indicates that the total flux of electric field through a closed surface is due to the density of charges. The equivalent of the Gauss law in magnetism in eq. (2.1.1d) shows that all the magnetic field lines are closed. Thus, magnetic monopoles cannot exist.

2.1.1 Electromagnetism and Maxwell equations in media

When changing from the vacuum to media the governing laws of electromagnetism change leading to a new version of them: the Maxwell laws in media. These can be obtained by considering some new magnitudes exclusive from the interaction of these fields with the media:

$$\boldsymbol{B} = \mu_0 (\boldsymbol{H} + \boldsymbol{M}) \tag{2.1.2}$$

$$\boldsymbol{D} = \boldsymbol{E} \cdot \epsilon_0 + \boldsymbol{P} \tag{2.1.3}$$

Where H is the magnetic field strength or external field and M the magnetization or the induced magnetic field. The latter magnitude is the response of the media to an applied field, so equation 2.1.2 shows that the total field or the magnetic flux B is the sum of the magnetic field strength or external field plus the magnetization of the media.

Similarly, with the case of the electric field 2.1.3, the applied field here is the old electric field E and the response of the material is the so-called polarization P. The sum of these two magnitudes leads to the electric displacement field D.

Finally, we have to reconsider the currents and density of charges. In vacuum all charges and currents were free but in media some charges will be intrinsic from the media and will be bounded ($\rho_{bounded}$). Some other charges are free and can move while there is electrostatic equilibrium, these are the ρ_{free} ; these two values sum up the whole charge density as seen in 2.1.5.

On the other hand, we have the case of the currents, the bounded currents are the ones caused by the electric and magnetic dipole moments of the elements in the media, the other currents will typically be named after free currents; in conclusion the free and the bounded currents in a media sum up to the total currents as seen in equation 2.1.4.

$$\boldsymbol{J} = \boldsymbol{J}_{free} + \boldsymbol{J}_{bounded} \tag{2.1.4}$$

$$\rho = \rho_{free} + \rho_{bounded} \tag{2.1.5}$$

By using the new magnitudes in media H, D and the current expressions we presented above we can get to the Maxwell laws in media, where the currents and charges that appear explicitly are only the free ones.

$$\nabla \times \mathbf{E} = -\frac{\partial \mathbf{B}}{\partial t} \tag{2.1.6a}$$

$$\nabla \times \boldsymbol{H} = \boldsymbol{J}_f + \frac{\partial \boldsymbol{D}}{\partial t}$$
 (2.1.6b)

$$\nabla \cdot \boldsymbol{D} = \rho_f \tag{2.1.6c}$$

$$\nabla \cdot \boldsymbol{B} = 0. \tag{2.1.6d}$$

Our study will focus on the interaction between magnetic fields and materials. Independently of the material the electromagnetic fields behave differently when entering a media than when they travel through vacuum. Both magnetic and electric fields have a similar behavior when interacting with materials but this thesis deals with magnetic fields so we will do the extended developments for the magnetic field case and later on, provide a summary of the same development for the electric field.

Starting with the magnetic case, let us suppose a case in which a magnetic field \boldsymbol{H} is applied in a region with a magnetic material. The media will react creating a magnetization \boldsymbol{M} , a local and macroscopic field that can be understood as the density of the microscopic magnetic dipolar moments:

$$\boldsymbol{B} = \mu_0(\boldsymbol{H} + \boldsymbol{M}); \tag{2.1.7}$$

Where we have the vacuum permeability $(\mu_0 = 4\pi \cdot 10^{-7} N/A^2)$ and **B** magnetic flux density. We can describe the curl of each of these fields as a current in the following way:

$$\mathbf{\nabla} \times \mathbf{H} = \mathbf{J}_f \quad \mathbf{\nabla} \times \mathbf{M} = \mathbf{J}_b.$$

So using these expressions and the curl of the magnetic induction field eq. (2.1.7) we obtain:

$$\nabla \times \boldsymbol{B} = \mu_0 (\boldsymbol{J}_f + \boldsymbol{J}_b); \tag{2.1.8}$$

Where J_f is the free current and J_b is the magnetization or bounded current. Now we can establish a relation between the magnetic field and the magnetization through the definition of magnetic susceptibility:

$$\boldsymbol{M} = \gamma_m \boldsymbol{H}. \tag{2.1.9}$$

This susceptibility shows the sensibility of the material against an external magnetic field; the larger the susceptibility, the larger the magnetization of the material due to the magnetic field. χ_m is usually defined as a scalar quantity in linear, isotropic, and homogeneous media but in general, it is a tensor that can change the modulus and direction of the magnetic field.

Now with this we can determine the magnetic induction field in terms of the magnetic field using eq. (2.1.9) and eq. (2.1.7):

$$B = \mu_0(H + M) = \mu_0(1 + \chi_m)H = \mu_0\mu_r H = \mu H; \qquad (2.1.10)$$

where μ_r and μ will also be tensors.

For the electric field, we have that similarly to the magnetic field, a dielectric material will have a response to an external field E called polarization P which is the vectorial macroscopic field coming from the density of electric dipoles:

$$\boldsymbol{D} = \epsilon_0 \boldsymbol{E} + \boldsymbol{P} \tag{2.1.11}$$

With $\epsilon_0 = 8.85 \cdot 10^{-12} F \cdot m^{-1}$ the vacuum permittivity. The electric displacement field \mathbf{D} can be understood as the external field applied. If we describe the density of charge as the divergences of the fields, we obtain

$$\nabla \cdot \boldsymbol{D} = \rho_f \quad \nabla \cdot \boldsymbol{P} = -\rho_b$$

Where the divergence of D only depends on the free charges ρ_f and the divergence of P depends on the bound charges ρ_b . Doing the same as in the magnetic fields we can express the divergence of the electric fields only in terms of free and bound charges:

$$\nabla \cdot \boldsymbol{E} = \frac{\rho_f + \rho_b}{\epsilon_0} \tag{2.1.12}$$

and similarly the electric susceptibility is:

$$\chi_e \epsilon_0 \mathbf{E} = \mathbf{P} \tag{2.1.13}$$

So we can rewrite the electric displacement field in terms of the electric field and the relative permittivity or the susceptibility, both of them tensorial and able to change direction and length of the electric field vectors:

$$D = \epsilon_0 \mathbf{E} + \epsilon_0 \gamma_e \mathbf{E} = \epsilon_0 (1 + \gamma_e) \mathbf{E} = \epsilon_0 \epsilon_r \mathbf{E} = \epsilon \mathbf{E}$$
 (2.1.14)

From the expressions derived above we can see that the final field \boldsymbol{B} (\boldsymbol{D} for the electric case) after the response of the material to the external fields \boldsymbol{H} (again \boldsymbol{E} for the electric derivation) is only depending on μ_r or ϵ_r so the final field will depend explicitly on the electromagnetic properties of the material.

2.1.2 Contour Conditions for the Electromagnetic Field

In our case we are also interested on the boundary conditions of the electromagnetic fields when changing from media. From López and Costa [2000] we can obtain these four conditions for the parallel and perpendicular components of each field between a media 1 and a media 2:

$$\hat{\boldsymbol{n}} \cdot (\boldsymbol{D_1} - \boldsymbol{D_2}) = \rho_s \tag{2.1.15}$$

$$\hat{\boldsymbol{n}} \cdot (\boldsymbol{B_1} - \boldsymbol{B_2}) = 0 \tag{2.1.16}$$

$$\hat{\boldsymbol{n}} \times (\boldsymbol{E_1} - \boldsymbol{E_2}) = 0 \tag{2.1.17}$$

$$\hat{\boldsymbol{n}} \times (\boldsymbol{H_1} - \boldsymbol{H_2}) = \boldsymbol{J_s} \tag{2.1.18}$$

These conditions for fields adjacent to perfect conductors can be rewritten into more compact and general boundary conditions when all fields in medium 2 are zero:

$$\hat{\boldsymbol{n}} \cdot \boldsymbol{B} = 0 \tag{2.1.19}$$

$$\hat{\boldsymbol{n}} \cdot \boldsymbol{D} = \rho_s \tag{2.1.20}$$

$$\hat{\boldsymbol{n}} \times \boldsymbol{E} = 0 \tag{2.1.21}$$

$$\hat{\boldsymbol{n}} \times \boldsymbol{H} = \boldsymbol{J_s} \tag{2.1.22}$$

These four boundary conditions state that magnetic fields can only be parallel to perfect conductors while electric fields can only be perpendicular. Moreover, the magnetic fields are always associated with surface currents flowing in orthogonal directions (with a numerical value equal to \mathbf{H}). Similarly, the perpendicular electric fields are always associated with a surface charge ρ_s numerically equal to \mathbf{D} .

2.2 Introduction to Superconductivity

Conduction is an intrinsic property of materials: all of them conduct but conductivity (σ) can vary from one extreme to another. A representative picture showing the wide range of conductivities (or resistivities) can be seen in figure 2.1 illustrating their variation by about 25 orders of magnitude from pure metals to ionic solids. On the one hand, some materials, such as glass or porcelain are almost perfect insulators leading to very few electrons flowing through. On the other hand, we have pure metals, such as gold, copper, and silver which appear to be very good conductors of electricity. This property can be defined as the material's ability to conduct electric current or a stream of charged particles such as electrons. In a more rigorous definition, it can be expressed as the ratio of the density of current (J) created by an electric field (E) to the same electric field at the particular point

$$\boldsymbol{J} = \sigma \boldsymbol{E} = \frac{1}{\rho} \boldsymbol{E} \tag{2.2.1}$$

According to Drude Hypothesis from Drude [1900], conduction electrons in a metal wander randomly in the distribution of positive ions fixed to their lattice positions. The ions can oscillate at a quantized frequency limited to the Debye or maximum frequency. Hence electrons will get scattered in this lattice in random directions leading to a mean drift equal to zero. The situation changes when an electric potential (ϕ) is applied. In this case electrons still get scattered by the ions but now a global drift appears in the opposite direction of the applied potential so a net current flows through the material.

Superconductivity is an electromagnetic phenomenon in which current flows without resistance in certain metals, alloys, and ceramics. Even if some metals can achieve very high conductivity (or low resistivity) a superconductor takes these properties to an extreme and has zero resistivity or infinite conductivity. Therefore a theoretical superconductor can carry a current indefinitely without losing any energy. However this phenomenon requires quite concrete conditions to appear.

The conditions that material needs in order to let electrons flow without resistance are

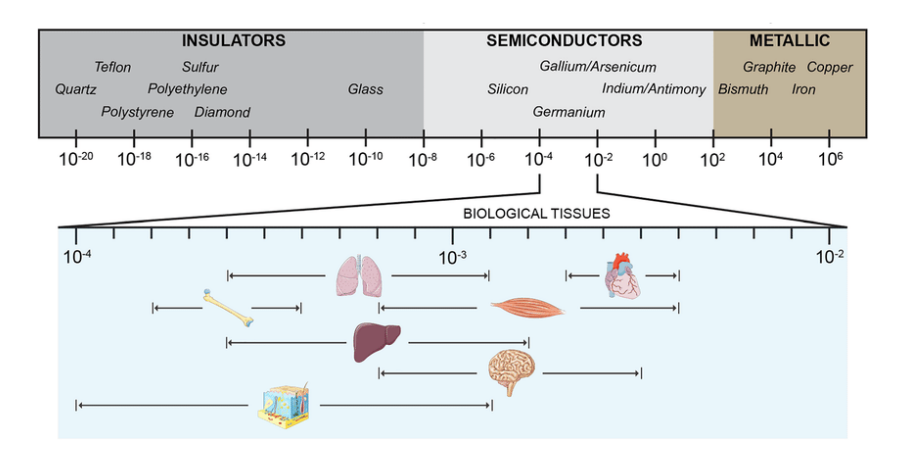


Figure 2.1: Scheme of conductivities of many materials from Solazzo et al. [2019]

given by several physical variables: The most relevant parameter for all superconductors is the critical temperature (T_c) , we also have the critical current density (J_c) and the critical magnetic field (B_c) . Above these critical quantities, the superconducting state is destroyed and the electrical current cannot flow without resistance.

2.2.1 Magnetic Shielding

Out of these phenomenon appear some consequent properties such as the Magnetic Shielding. This Shielding is the ability of superconductors to expel the magnetic field lines. In this section we will go through this phenomenon explaining how it works and why it happens in superconductors.

Let's first consider two identical cylinders of radius a that are infinitely long. One of the cylinders will be a perfect conductor with a temperature close to 0K and the other will be a superconductor cylinder at a temperature $T < T_c$. To both cylinders, an external field \boldsymbol{B} is applied in a parallel direction to the cylinder axis.

If we take into account the Faraday law in 2.1.1a calculating the line integral over a closed line in a plane perpendicular to the field we have:

$$\int \mathbf{E} \cdot d\mathbf{l} = -\frac{d}{dt} \int \mathbf{B} \cdot \mathbf{n} \ dS = IR = 0$$
 (2.2.2)

It is known that the resistivity is zero in both cylinders which leads to a zero temporal variation of the magnetic flux. If not, infinite currents would be generated in the plane and we know it is not possible.

Since we applied an external field \boldsymbol{B} , in order to have an internal zero-field variation, circular currents will appear in the materials compensating the external field. As a result of this setup, if we started with a zero field then the variation will always be zero and so the field will be excluded from the inside of the cylinders, or what is the same:

$$\mathbf{B} = \mu_0(\mathbf{H} + \mathbf{M}) = 0 \tag{2.2.3}$$

So $\mathbf{H} = -\mathbf{M}$ which leads to a susceptibility $\chi = -1$, indicating that both superconductor and perfect conductor act as a perfect diamagnetic material. This is just in a purely theoretical and perfect case where the current density of the superconductor is infinite, but we will see in the chapter 4 how a finite J_c allows the field to enter the material and also have currents inside the material. But still, in this perfect case, the currents generated can only be superficial, if not we could apply the $Amp\acute{e}re~law~2.1.1b$ in a closed line inside the material leading to a non-zero field which we know is not possible.

This phenomenon is called **magnetic shielding** and it is a key characteristic of the zero resistance materials. For the moment we would have the same scenario for both the perfect conductor and the superconductor, which will not happen in the **Meissner-Ochsenfeld effect** described below.

Meissner-Ochsenfeld Effect

Magnetic shielding is a property that could be achieved by both conductors and superconductors, but the Meissner-Ochsenfeld Effect is only possible in superconductors. The Meissner-Ochsenfeld effect is the expulsion of a magnetic field from a superconductor during its transition to the superconducting state when it is cooled below the critical temperature. The different ways this phenomenon shows up is the basic feature for classify the superconductors in terms of the critical field. Let's consider again the same set up of the previous section, with both cylinders of a superconductor and a perfect conductor, but now in different conditions: the perfect conductor at a temperature T > 0K and in consequence with a resistance different from zero. The superconductor at a temperature over the critical temperature and therefore in the resistive state.

Now we apply a field B lower than the critical field and start to decrease gradually the temperature. At the point we cross the critical temperature (T_c) the superconductor will suddenly generate surface currents turning the inner field to zero; this happens without having any variation of the magnetic flux. Thus this expulsion of field lines cannot be justified by the Faraday Induction law because there has not been any field variation but a temperature variation.

Now we could do the same procedure with the perfect conductor cylinder decreasing the temperature to 0K but the inner field will remain the same as the outer one. That is, in this case, the field will penetrate the material without generating any current.

We have this situation because in the perfect conductor the field \boldsymbol{B} can only be excluded by $Faraday\ Induction\ law$ but this can never be due to the Meissner-Ochsenfeld effect.

After this, we can now classify the superconductors according to the way they expel the magnetic field lines and their critical magnetic field.

 $^{^{1}}$ A diamagnetic material is defined as a material that under an external field \boldsymbol{H} generates a field \boldsymbol{M} opposed to this external field

2.3 Superconductor classification

This phenomenon can look simple from a theoretical point of view when we observe it from a practical or more real view we observe that it is very complex and there are lots of types of superconductors, each of them with some special features. In this thesis we will focus on two main classifications, one regarding the different behaviors of these materials with the critical fields \mathbf{H}_c and the other focusing on the characteristics of the critical temperature T_c .

2.3.1 Critical Magnetic Field Criterion

One possibility to classify the superconductors is depending on the critical magnetic field. Behind the zero-resistance concept there are many physical implications, one of the most relevant is the complete expulsion of the magnetic field of the material, also called the **Meissner-Ochsenfeld effect** explained in previous sections (section 2.2.1).

Depending on how the superconductor expels the magnetic field lines, it can be classified in two main types.

Type-I Superconductors

The first type of superconductors are known to have just one critical field H_c . For this type we have an abrupt change from being below this field, where we have the superconductor state and the complete expulsion of the field lines, to the normal conductor state.

This type of superconductor is the closest to the theoretically presented before. Below the critical temperature it presents a critical field H_c and its behavior is described by the Meissner-Ochsenfeld effect, but above this critical field the diamagnetic behavior is lost and it acquires the typical conductor behavior. Typically these superconductors have very low H_c (of the order of mT), such as the metallic Mercury. That is why they are not very relevant for applications where they need to resist strong currents and fields. In these cases, they would be always over the critical field and so they would behave as normal conductors.

Type-II Superconductors

On the other hand, for Type-II Superconductors the typical critical field unfolds in two critical fields $(\boldsymbol{H_{c1}}, \boldsymbol{H_{c2}})$ developing an intermediate phase of the mixed ordinary and superconducting properties. So now the superconductor can be in three regimes:

- $H < H_{c1}$ In this state or phase the superconductor behaves like a typical Type-I superconductor by showing a Meissner-Ochsenfeld effect and expelling all the magnetic flux out of the material.
- $H_{c1} < H < H_{c2}$ When a Type-II superconductor is in this region we can observe a mixed state between a Type-I superconductor and a normal conductor. Some magnetic field lines will penetrate the material and get pinned forming magnetic field vortices.

These vortices, also called *Abrikosov vortices*, are vortices of supercurrent around an amount of magnetic flux.

One interesting property of these vortices is the fact that they obey London's magnetic flux quantization and carry one quantum of magnetic flux Φ_0 . So when increasing the external magnetic field the amount of magnetic field in a vortex will not change but new vortices will appear carrying all of them the same quantization of flux.

By adding defects on the superconductor these vortices can be pinned in certain locations making the magnetic field to go through those particular places.

For further documentation regarding London magnetic flux quantization see London and London [1935].

• $H > H_{c2}$ When the field is higher than the second critical field the material has no longer a superconducting behavior and it just becomes a resistive conductor. This state is similar to the Type-I superconductors when increasing the field over the H_c .

In the case of some Type-II superconductors, we have to take into account another physical parameter that might affect the superconducting state such as the strain ϵ .

For example, HTS tapes that need to carry large amounts of the current need to be Type-II superconductors. The behavior of these tapes relies very much upon the crystalline shape of the material. Thus the strain dependence is easily understood by assuming that at some point this strain will change the structure of the metal causing it to lose the superconducting state. Besides that, many of the applications for which they are expected to work would be in extreme conditions with high-intensity fields and hence forces will appear that can stress the materials to a point where superconductivity is not held.

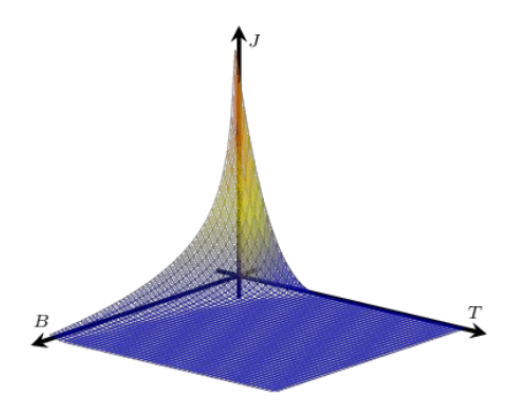


Figure 2.2: Example of Critical Surface by Lorenzo [2019].

 B_c, T_c, ϵ depend on each other so the superconductive state is delimited by a *Critical Surface*. Hence having the superconductor material below this surface will lead to a superconducting state, and on the other hand, having it over the surface will turn the material into a normal conductor with a non-zero resistivity.

Concretely the case of Type-II superconductors has been widely studied because unlike Type-I Superconductors, the second critical field B_{c2} for some of these superconductors can reach values between 10 to 20 Tesla.

This leads to a large number of applications, and because of having larger values of B_{c2} and often T_c the critical surface becomes very important in order to know in which conditions they will be under the superconducting state. That is why is often modelled as a product of separable functions as it follows:

$$J_c = J_c(T, B, \epsilon) = \frac{C}{B}g(\epsilon)h(t)f_P(b), \qquad b = \frac{B}{B_{c2}(T, \epsilon)}$$
(2.3.1)

2.3.2 Critical Temperature Criterion

Superconductors can also be divided into two main groups according to their Critical Temperature. This criterion is mostly related to the coolant itself. In the beginning, the first superconductors as Hg or Sn were showing this special behavior when cooled down to temperatures close to 0K (for example in the case of Mercury with $T_c \approx 4K$) but recently many ceramics have been discovered with critical temperatures over 70K. In figure 2.3 all the cases above liquid Nitrogen are High-Temperature Superconductors and all the ones below are Low-Temperature Superconductors.

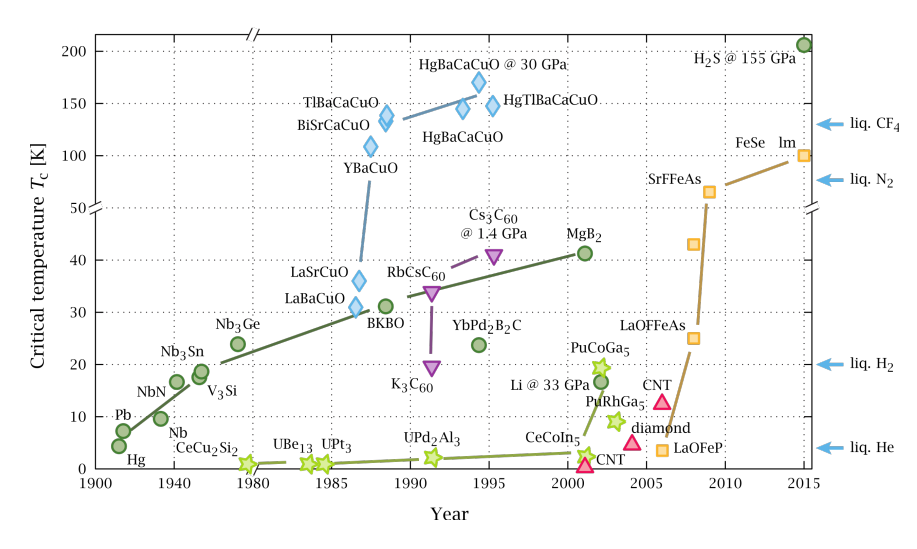


Figure 2.3: Scheme of some Superconductors by its composition, Critical Temperature and Year of discovery by PJRay, Wikipedia [19 November 2015]

Low Temperature Superconductors

Low-Temperature Superconductors are mainly metals and alloys, they were the first to be discovered by Delft [2012] and they need liquid Helium to be cooled down to these temperatures. This feature makes them expensive to maintain and so they were mainly used for scientific experiments. Its cost does not allow them to be used on a continuous or on a large scale because the amount of liquid Helium needed makes it unfeasible. Some examples of these superconductors are metallic Mercury with $T_c \approx 4K$ or alloys like Nb_3Sn working in the range of 6-18K

High-Temperature Superconductors

In addition to Low Temperature Superconductors, we have High-Temperature Superconductors (HTS), which are the type of Superconductors simulated using the magnet module in chapter 4. These kinds of superconductors have a substantially higher critical temperature. In particular, the boundary temperature between HTS and Low-Temperature Superconductors is at 77K, the boiling point of liquid nitrogen.

This is due to the fact that at 77K is the temperature achievable by liquid Nitrogen. Liquid Nitrogen is cheaper and easier to obtain than liquid Helium. Hence cooling with Nitrogen instead of Helium makes superconductors more competitive and possible to use in a more generalised way (Low-Temperature Superconductors are mostly used in big companies or institutions that can afford the high cost of using them). The lower boundary at 77K does not mean however that we can have HTS working at room conditions (temperature and pressure). They actually work well only below the lowest atmospheric temperatures recorded on Earth so they all still require a cooling system. HTS are usually ceramic materials and this leads to some drawbacks. Ceramics are brittle and so the fabrication of wires becomes quite problematic. The main classes are copper oxides and some iron-based compounds.

As a curiosity, some extremely-high pressured superhydride compounds achieved superconductivity at really high temperatures. At the moment the record holder is a carbonaceous sulfur hydride being able to hold superconductivity until a temperature of 15 °C as reported by Huang et al. [2019]. Despite this high temperature, it should be noticed that the conditions in which the superconductivity is held are not common conditions, in fact, a pressure around 267 GPa is required, which is almost the pressure at the Earth's core.

2.4 Applications for Superconductors

Superconductors have shown to be very useful materials when trying to carry large amounts of current without having losses or when trying to expel or pin some magnetic fields out of the material.

The electricity that powers most of the devices always encounters resistance which converts part of the energy into heat. This is the main cause for deterioration or energy loss and, except for some devices like toasters or stoves, this heat is an unwanted phenomenon wasting energy and damaging devices. As said before the main drawback of superconductors is their cost and the fact that they need to operate in very low temperatures so for the moment the applications are limited to scientific experiments or state-of-the-art technology.

For example, they are used in high-energy particle accelerators, concretely in wires that need to carry large amounts of current like CERN electromagnets. It is expected to use them in fusion reactors like ITER also to create big magnetic fields to confine the plasma.

In Japan and Germany, there are some experiments in order to build superconducting magnets that lift experimental levitation trains above rails in order to eliminate friction.

Moreover, they have been used experimentally to speed up connections between computer chips, also for superconducting coils making possible the powerful electromagnets to work in some of the magnetic resonance imaging (MRI) machines used by doctors to examine soft tissue inside patients.

As we can see, superconductors are state-of-the-art technology that is already used in many fields and seem to be very promising but is still under development for further applications. That is why they need lots of work and experiments before they can get to general use or at least a more extended usage.

2.4.1 Quench in superconductor tapes

As we could see in the previous section superconductors may be very useful for situations in which big amounts of current need to be transported. Hence we can create extremely strong electromagnets without having big losses. Nevertheless, there are not only good news regarding superconductors because their state and behavior are unstable and susceptible to environmental changes.

As a simple example, if the current flowing through a tape is a bit higher than the critical current or if the temperature of the superconductor slightly rises above the critical temperature the superconducting state will be lost in some parts of the tape. This will cause energy dissipation, this dissipation will increase the temperature of the surroundings and more volume of the tape will move from the superconducting state to a resistive state.

This variation will trigger a chain reaction along the superconductor causing it to lose the superconductor state and generating large energy dissipation. This phenomenon is the so-called *Quench* and has dramatic consequences to the superconductors. The energy dissipation is so high that can bring the superconductor to very high temperatures and cause severe damages to the material and to the other devices surrounding it. If there are no strategies to avoid these chain reactions this situation will bring the system to a point that an emergency shut down will be necessary in order to cool down the superconductor and it will take a while to restart the whole system and have it ready to start again.

As can be seen, a *Quench* is a situation that can happen quite frequently in superconductors with large currents flowing through them. It needs to be studied and monitored so these situations can be avoided or at least foreseen before they are about to be triggered. This thesis is a part of a research line that aims to develop a HPC multiphysics code able to study these *Quench* situations without the need to do real experiments wasting superconductors and big amounts of coolant.

2.5 Superconductor Modelling

After going through the theory of superconductivity this section focuses on the modelling of superconductivity. Predicting accurately and efficiently the magnetic response of high-temperature superconductors is of high importance in numerous applications such as energy transport and storage, trapped-field magnets, or magnetic shielding.

Numerical models related to the study of electromagnetic behavior of HTS have seen a booming expansion in recent years thanks to the fact that the technology related to them is becoming more mature with many applications in the precommercial stage. This is related to the demand for tools able to optimize their design and reliability as well as the need to be able to predict their performance.

However, the behavior of HTS is not easy to simulate, especially when coming to applications with time-varying magnetic fields. This analysis can be done analytically to a certain extent, but usually, these models are limited to simple materials and geometries.

The situation gets even more complicated when there is a need to take into account the dependence of critical current density J_c on the magnetic field B, temperature, or strain.

Many formulations for simulating electromagnetic problems have arisen from the Maxwell laws depending on the needs and the problem to solve. Usually, when trying to solve these problems the technique does not consist of solving the Maxwell laws explicitly but using a formulation of these laws in terms of concrete variables (electric or magnetic fields as well as potentials). All of them have advantages and drawbacks depending on the problem itself.

In the next sections we will go through different formulations used for simulate electromagnetic problems and finally we will deepen on the H-formulation, the one used in the magnet module of Alya.

$T - \phi$ Formulation

The first formulation was proposed by Amemiya et al. [1998] in 1998 in order to calculate AC losses in a variety of working conditions. This formulation, based on the finite element method, was a 2-D $T - \phi$ formulation of the Maxwell laws. The $T - \phi$ formulation (also called Torque formulation) uses the following definitions applied on the Maxwell laws:

$$egin{aligned} oldsymbol{J} &=
abla imes oldsymbol{T} \ oldsymbol{H} &= oldsymbol{T} -
abla \phi \
ho &=
ho(J) \end{aligned}$$

Where T is the magnetic torque and ϕ the electric potential.

By knowing these three definitions and using some of the relations with the Maxwell laws, we obtain the $T - \phi$ formulation that is the following:

$$\nabla \times \rho \nabla \times \mathbf{T} = -\mu \frac{\partial \mathbf{T} - \nabla \phi}{\partial t}$$

$$\nabla^2 \phi = 0$$
(2.5.1)
(2.5.2)

$$\nabla^2 \phi = 0 \tag{2.5.2}$$

A - V Formulation

Two years after at the Polytechnique Grenoble tested different formulations with superconductors and successfully developed a module based on the A-V formulation (for further information see Vinot et al. [2000]). This formulation used the next expressions in

the Maxwell laws:

$$\begin{aligned} \boldsymbol{B} &= \nabla \times \boldsymbol{A} \\ \boldsymbol{E} &= -\frac{\partial \boldsymbol{A}}{\partial t} - \nabla V \\ \boldsymbol{\sigma} &= \boldsymbol{\sigma}(\boldsymbol{E}) \end{aligned}$$

where \boldsymbol{A} is the magnetic potential. With this we can rewrite the Maxwell Equations in these two expressions that represent the $\boldsymbol{A}-V$ formulation:

$$\nabla^2 \mathbf{A} = \mu \sigma \left(\frac{\partial \mathbf{A}}{\partial t} + \nabla V \right) \tag{2.5.3}$$

$$\nabla \cdot \left(\sigma \frac{\partial \mathbf{A}}{\partial t} + \sigma \nabla V \right) = 0 \tag{2.5.4}$$

E-Field Formulation

Finally we have the two formulations based on the fields governing the Electromagnetism. First we will focus on the E - field formulation, which similarly uses definitions:

$$\frac{\partial \mathbf{B}}{\partial t} = -\nabla \times \mathbf{E}$$
$$\sigma = \sigma(\mathbf{E})$$

and combines the Maxwell laws using some vector identities together with these expressions to obtain the $\mathbf{E} - field$ formulation:

$$\nabla \times \nabla \times \mathbf{E} = -\mu \frac{\partial \sigma \mathbf{E}}{\partial t} \tag{2.5.5}$$

This formulation uses as a variable the Electric field and can be very useful when the variable to study is this field.

All these formulations and other recent ways to model HTS can be found in the articles Dular et al. [2020] or Grilli [2016]

H formulation

The H-field formulation takes its name from the single dependent variable of magnetic field intensity H. It was first used to calculate macroscopic current and field distribution in research codes such as the one mentioned in Pecher et al. [2003] but afterwards it was implemented in commercial finite element method software such as COMSOL in Hong et al. [2006] or Grilli [2016]. It has been used for modeling many HTS topologies with the advantages of accuracy, good convergence, and acceptable computing time. Furthermore it is the formulation used in the magnet module in Alya so the one we will be using for the simulations.

Mathematically the \mathbf{H} formulation rewrites the Maxwell laws in a form that solves the Faraday's law 2.1.6a using the magnetic field \mathbf{H} as a state variable and a nonlinear resistivity

for describing the characteristic electrical behavior of superconductors 2.5.7. Recalling that it uses the Faraday law in terms of the vector \mathbf{H} we can obtain the expression for the formulation using the fact that $\mathbf{B} = \mu \mathbf{H}$ with $\mu = \mu_r \mu_0$. Furthermore knowing that the lower critical field below which type-II superconductors are in the Meissner state is usually very low (mT range) in most practical cases of power applications, one can assume $\mu_r = 1$ for the superconductor material. Since $\mathbf{E} = \rho \mathbf{J}$ and $\mathbf{J} = \nabla \times \mathbf{H}$ we can rewrite the Faraday's law in the following way:

$$\nabla \times \mathbf{E} = -\frac{\partial \mathbf{B}}{\partial t}$$

$$\nabla \times \rho \mathbf{J} = -\frac{\partial \mu \mathbf{H}}{\partial t}$$

$$\nabla \times \rho (\nabla \times \mathbf{H}) = -\frac{\partial \mu \mathbf{H}}{\partial t}$$

$$\frac{\partial \mu \mathbf{H}}{\partial t} + \nabla \times (\rho \nabla \times \mathbf{H}) = 0$$
(2.5.6)

From this derivation we reached the \mathbf{H} -formulation expression (equation 2.5.6) and as we see we will be solving a Finite Element problem where the problem variable is a variable of interest for our study (\mathbf{H}). Another interesting property is that this formulation allows to fix the field as contour conditions and has explicitly the resistivity.

The magnet module of Alya will use the Finite Element method to solve the problem of the H-formulation using the last expression we reached, and also has the possibility to use constant resistivity or the power-law expression we will present on section 2.5.1.

2.5.1 Modelling the Resistivity

The superconductors are modeled as materials with nonlinear electric resistivity, usually in the form of a power law as seen below

$$\rho = \frac{E_c}{J_c(T, \mathbf{B}, \epsilon)} \left| \frac{\mathbf{J}}{J_c(T, \mathbf{B}, \epsilon)} \right|^{n-1}$$
(2.5.7)

This modelling of the resistivity has E_0 as the characteristic electric field (generally $10^{-4} \ V/m$), J the current density and J_c the critical current density. Finally, n is a parameter that indicates the steepness of the transition from the superconducting to the normal state. In Alya's magnet module the law is implemented to calculate the resistivity. In particular the default values for the constants are:

$$E_c = 0.0001 \ V/m$$
$$J_c = 1 \cdot 10^8 \ A/m^2$$
$$n = 30$$

These values were changed during the simulations, concretely in the magnetic field dependent Critical Current density (explained in Section subsection 4.2.4) the value obtained for J_c was inserted here.

Such a nonlinear resistivity mirrors also the nonlinear voltage-current relationship where the critical current I_c is the density of current times the section of the tape $I_c = J_c \cdot S$, and it is the current at which a threshold voltage is reached.

In general, and also in our cases, J_c depends on the magnetic field, amplitude, and the angle of this field with respect to the material. This dependence can assume fairly complicated forms. One of our goals in chapter 4 will be to model these dependencies. This power law is commonly used to describe power dissipation at power frequencies. For slower phenomena, as relaxation² the percolation law given by Strelniker et al. [2007] which can give a more accurate description. The non-conducting materials are modelled as media with high resistivity; usually, $1 \Omega m$ is sufficiently large to avoid the flow of current in non-conducting regions, but high resistivities lead to convergence problems and increase the computation time.

2.5.2 Biot-Savart Law for the Self Field Option

In our model, we use an option called Self Field to calculate the magnetic field in each point depending on the current on all the points. The general law in integral form is the following:

$$\boldsymbol{B}(\boldsymbol{r}) = \frac{\mu_0}{4\pi} \iiint_V \frac{(\boldsymbol{J}dV) \times r'}{|\boldsymbol{r'}|^3}$$
 (2.5.8)

This formulation from López and Costa [2000] is the general version of the Biot Savart law for conductors with finite width. Here r' is the vector from dV to the observation point r, dV is the volume element, and J is the current density vector in that volume. With this law, the field can be computed at each point only by knowing the current distribution in the domain. When the Self-Field option is activated the magnetic field in the subdomain required will be calculated by going through all the edges and calculating the integral 2.5.8. With this, we can reduce substantially the air domain.

²Further we will see how the Alya code has problems when simulating relaxation due to the fact that uses this power-law resistivity.

Chapter 3

The Finite Element Method Alya Code

Alya is a High-Performance Computing code developed at Barcelona Supercomputing Center (more information can be found in CASE department [2021]). It is used to solve problems with large meshes and complex boundary conditions.

It is mostly written in FORTRAN and it uses MPI parallelization techniques in order to adapt to supercomputers with large amounts of processors. The preferred domain discretization technique in Alya is the Finite Element Method, which is the one that will be used in this Thesis simulations.

In this chapter we will go briefly through the theory regarding the Finite Element Method, later on, we will give a description of what is Alya. Afterward, we will focus on the structure of Alya and last of all a first in detail explanation of magnet will be done, the module used in this thesis to do the simulations.

3.1 The Finite Element Method

First of all our aim is to give a brief summary of how the Finite Element Method works. We will not go through rigorous developments nor deep explanations of the topic since a general description of this topic will be enough in order to understand the theoretical basis upon which Alya is built. For a more advanced description and better understanding of the topic refer to Kuzmin and Hämäläinen [2014].

The Finite Element Method (from now on FEM) is a method based on a variational form of the differential equation. In general, it is a numerical method for solving a PDE in two or three space variables. To solve the problem the method subdivides the whole domain into smaller simpler parts called **finite elements**. This step is done by constructing a mesh of the object. Hence the finite element method formulation of a boundary value problem results in a system of algebraic equations.

Thereupon an approximation of the unknown function over the domain is done and the simple equations that model these finite elements are assembled into a large system of equations modelling the entire problem.

3.1.1 Technical Overview of FEM

The Finite Element Method can work for many PDE or many dimensions but in order to make a simpler overview of how the system of equations is built out of the PDE we will consider a simple 1-D problem to depict the various stages involved in the Finite Element Analysis.

The first step is to identify the PDE associated with the physical phenomenon. In our thesis, the PDE is the \mathbf{H} -Formulation equation 2.5 also known as the strong form and the integral form which is known as the weak form. We will go through an example in order to explain how this Finite Element Method goes from a PDE to a system of equations. First of all we will consider the PDE u''(x) = f(x) in the domain [0,1].

$$u''(x) = f(x)$$
$$\int u''(x)v(x) = \int f(x)v(x)$$

By considering the PDE presented before, we can turn it into an integral form or weak form. The equation is multiplied by a trial function v(x). Hence by integrating by parts the above equation can be rewritten as:

$$u'(x)v(x)\big|_0^1 - \int u'(x)v'(x) = \int f(x)v(x)$$
 (3.1.1)

As it can be seen, the advantage of using the weak form is that the earlier differential equation required u(x) to be two times differentiable while this weak form only requires it to be differentiable once. An analogous procedure can be followed for problems posed in higher dimensions by replacing the derivatives with gradients and divergences.

Once the weak form is set up the following step is to find a finite subspace belonging to the solution for the weak formulation. With this, we can go from a problem from an infinite space to a finite number of points where we can find the solution numerically. Besides this, another goal of discretization is to convert the integral form into a set of matrix equations that are more easily solvable by using well-known theories of matrix algebra. Given the fact that this expression needs to be solved numerically, this integration is converted to a summation calculated numerically.

The domain now is divided into small pieces according to the mesh presented in the beginning, the pieces will be called "elements" and for low order elements the corner points of each element will be known as "nodes"; in general elements, the nodes do not need to coincide with the vertices, in quadratic elements. For example, the nodes can be in the center of the edges or inside the element. Typically the degrees of freedom u_i are assigned to the mesh nodes, but in the Finite Element method used in this work, the Degrees of Freedom are assigned to the mesh edges. For simplicity, we will do the derivation for nodal calculations while knowing that in some cases we will use in fact edge-calculations.

Interpolation functions are defined for each element, and hence the value inside the element can be calculated by using the value on the nodes. These functions are often referred

to as ansatz functions. Thus the new approximated solution is expressed as:

$$u(x) = \sum_{n=1}^{\#nodes} N_i u_i$$

where the functional will be summed for all the nodes, N_i is the interpolation function, and u_i is the unknown, both associated to the node i. Similarly to the case of the u(x) the interpolation can be used for the two other functions f(x) and v(x). Now we can rewrite the equation 3.1.1 of the weak form in terms of these summations in the following way:

$$\left(\sum_{n=1}^{\# nodes} N_{i}u_{i}\right)' \left(\sum_{n=1}^{\# nodes} N_{i}v_{i}\right) \Big|_{0}^{1} - \int \left(\sum_{n=1}^{\# nodes} N_{i}u_{i}\right)' \left(\sum_{n=1}^{\# nodes} N_{i}v_{i}\right)' = \int \left(\sum_{n=1}^{\# nodes} N_{i}f_{i}\right) \left(\sum_{n=1}^{\# nodes} N_{i}v_{i}\right) \\
\left(\sum_{n=1}^{\# nodes} N'_{i}u_{i}\right) \left(\sum_{n=1}^{\# nodes} N_{i}v_{i}\right) \Big|_{0}^{1} - \int \left(\sum_{n=1}^{\# nodes} N'_{i}u_{i}\right) \left(\sum_{n=1}^{\# nodes} N'_{i}v_{i}\right) = \int \left(\sum_{n=1}^{\# nodes} N_{i}f_{i}\right) \left(\sum_{n=1}^{\# nodes} N_{i}v_{i}\right) \\
\int \left(\sum_{n=1}^{\# nodes} N_{i}f_{i}\right) \left(\sum_{n=1}^{\# nodes} N_{i}v_{i}\right) = \int \left(\sum_{n=1}^{\# nodes} N_{i}f_{i}\right) \left(\sum_{n=1}^{\# nodes} N_{i}v_{i}\right) \\
\int \left(\sum_{n=1}^{\# nodes} N_{i}v_{i}\right) \left(\sum_{n=1}^{\# nodes} N_{i$$

The summations can be rewritten as matrix products with vectors according to this expression:

$$\sum_{n=1}^{m} N_i u_i = \mathbb{M} \cdot \boldsymbol{u} \tag{3.1.2}$$

where u_i is the set of unknowns and N_i the ansatz functions. Hence we can rewrite all the weak form with summations in terms of matrix multiplications using the expression

$$\boldsymbol{v}^{T} \cdot \left(\mathbb{M}^{T}\mathbb{M}'\right)\Big|_{0}^{1} \cdot \boldsymbol{u} - \boldsymbol{v}^{T} \cdot \left(\int \mathbb{M}'^{T}\mathbb{M}'\right) \cdot \boldsymbol{u} = \boldsymbol{v}^{T} \cdot \left(\int \mathbb{M}^{T}\mathbb{M} \cdot \boldsymbol{f}\right)$$
(3.1.3)

With this expression we can remove the trial function v(x) since its multiplying to all the terms and it has to be fulfilled for any v(x). Finally, we can rewrite the whole weak form into a matrix form:

$$\left\{ \left(\mathbb{M}^T \mathbb{M}' \right) \middle|_0^1 - \left(\int \mathbb{M}'^T \mathbb{M}' \right) \right\} \cdot \boldsymbol{u} = \left(\int \mathbb{M}^T \mathbb{M} \cdot \boldsymbol{f} \right)$$
(3.1.4)

 $\mathbb{A} \cdot \boldsymbol{u} = \boldsymbol{b} \tag{3.1.5}$

In conclusion, we achieved to turn the PDE into a matrix form. This last step packed the first bracket into the matrix \mathbb{A} called the stiffness matrix and the right side parenthesis into the vector \boldsymbol{b} called the residual vector. The unknowns are packed into the vector \boldsymbol{u} called the nodal unknowns.

One point we did not go through is the interpolation functions. The mathematics involved in the decision of these functions usually requires functional spaces. In this thesis we will not go in detail on that choice because it is out of its scope. For further information regarding FEM view Bofang [2018] Now the only remaining issue that still needs to be done is to solve this system of equations, in the case of Alya the algorithm used is the Preconditioned Conjugate Gradient Method.

The weak form presented in 3.1.5 is the system of equations for the PDE u''(x) = f(x) while our PDE to solve is the H-Formulation expression, which in differential form is:

$$\frac{\partial \mu \boldsymbol{H}}{\partial t} + \nabla \times (\rho \nabla \times \boldsymbol{H}) = 0$$

After some developments explained in Lorenzo [2019], we obtain the weak form for this PDE where the unknown function is $\mathbf{H} \in \mathcal{H}_D(\boldsymbol{curl}, \Omega)$ such that:

$$\frac{d}{dt} \int_{\Omega} (\mu \boldsymbol{H}) \cdot \boldsymbol{v} d\Omega + \int_{\Omega} (\rho \nabla \times \boldsymbol{H}) \cdot (\nabla \times \boldsymbol{v}) d\Omega = -\int_{\Gamma_N} \boldsymbol{g}_N \cdot \boldsymbol{v} d\Gamma, \ \forall \boldsymbol{v} \in \mathcal{H}_0(\boldsymbol{curl}, \Omega)$$
(3.1.6)

In our work, we will only consider the Dirichlet boundary conditions so the right hand side of the expression will vanish. Dirichlet boundary conditions specify the values that a solution needs to take along the boundary of the domain, for further information check simscale.com [accessed: February 9, 2022]. The \mathcal{H}_D is the function space such as the L2 norm of the rotational of \boldsymbol{v} is bounded.

Differently from the case presented above, the H formulation weak form in the magnet module uses edge elements instead of node elements to approximate the final solution.

The issue of choosing the finite subspace in which the solution is searched depends on the problem itself. In the case of the magnet module, the subspace chosen is the edge subspace because it needs to belong to $H(\boldsymbol{curl}, \Omega)$.

3.2 Overview of Alya Code

Alya is a simulation code developed since 2004 mainly by Guillaume Hozeaux and Mariano Vázquez. It is not a born-sequential simulation code parallelized afterward but it was designed from scratch as a multi-physics parallel code.

It solves discretized PDEs by using the Finite Element Method. The space discretization used is based on unstructured meshes, with several types of elements such as pyramids, tetrahedrons, etc. It has both explicit and implicit time advanced schemes and depending on the case, staggered or monolithic schemes are programmed to address the solution of multi-physics problems. However, for large multi-physics problems, the preferred schemes are staggered with coupling iterations.

Regarding the parallelization, Alya is based on mesh partitioning using the third-party library METIS from Karypis [accessed: February 9, 2022] and MPI tasks, techniques that work very well with distributed-memory machines. On top of this, some heavy-weight loops are parallelized with OpenMP threads. Both layers can be used at the same time in a hybrid

scheme. Another advantage of Alya is the fact that it has sparse linear algebra solvers specifically developed for it, with a tight integration with the overall parallelization scheme. Hence third-parties solver libraries are not required. It can be linked to other external solvers like MUMPs (further information regarding MUMPs can be found in MUMPs [accessed: February 9, 2022]). Furthermore, Alya includes geometrical tools which operate on the meshes to smooth, decompose the domains or subdivide the meshes. This tool is very useful for large-scale simulations.

Alya is organized in a modular structure with a Kernel handling the domain partitioning and algebra parallelization. In addition to this, the kernel also nests common linear algebra operations and linear solvers such as the Conjugate Gradient Method, an iterative method for solving linear systems with SPD matrices based in the Krylov subspaces (explained more in detail in Saad [2003]), also it has preconditioners for the linear systems so you can focus on the physical problem.

Each module solves a particular physical problem, such as the neutro module modelling neutron flux, the turbul for turbulence, and solidz for Solid Mechanics.

Apart from this, the Alya system consists of a number of services. They are procedures that can be used by different modules and the kernel. Examples of services are the codes of parallelization and optimization techniques.

3.3 Main Structure of Alya

After the brief summary of Alya we will focus on its structure. Alya structure from the root is conformed by the following folders:

- Sources
- Executables
- Utils
- src
- Config

Apart from them, there are other folders for testing or for third-party software together with the Licenses and cmake archives to execute parts of the code. Out of the general structure of the Alya code, what concerns us the most is the Sources folder and the Executables folder, the others are just used to build up the Alya code and have routines that should not be modified.

If we begin with the folder Executables/unix it stores different executables out of the Fortran scripts, any time we modify anything from the Alya code we need to go to this directory and input make all to recompile the updated codes. Afterwards, we have the main folder /Sources with the three main parts of Alya, first, the Sources/Alya folder

containing many basic subroutines of Alya itself like the core, the one responsible for the parallelization, or for the operations of matrices.

Then we have the Sources/kernel explained before and finally the Sources/modules folder, containing all Alya modules and their subroutines. In case of needing to modify any parameter or, as we will see afterwards, contour or initial conditions, we will need to change it in the modules folder.

- Read Files, def. mesh dependent arrays - Initial solution or read restart - Output and postprocess do time steps - Compute time step - Begin a time step: update bc, etc. do blocks Modules are grouped into blocks do coupling Useful if some equations are coupled and others - Solve module1 decoupled. Example: - Solve module2 Block 1: Nastin - Turbul Block 2: Chemic: species are transported - Check coupling cvg end do coupling Goto new block end do blocks - End time step - Output and postprocess - end do time step - Output and postprocess - End the run

Figure 3.1: General Workflow of the Alya system from CASE department [2021]

A scheme of Alya's workflow is presented in figure 3.1. The inner loops correspond to the coupled modules, depending on if the modules coupled are from the same block (physically coupled or with some equations coupled) or from different blocks. However, the outer loop corresponds to the time iterations. The interesting part of these modules is that they can be coupled and run simultaneously in order to solve the different physics of a single problem. We have many modules focused on physical problems such as nastin which simulates Navier-Stokes equations for incompressible gases, nastal for compressible gases, chemic for simulating chemical reactions, turbul for modelling turbulence in gas, also solidz which simulates solid-state problems, neutro for neutronics simulations and finally the ones concerning us the most are the magnet module and, for further work out of this thesis, the temper module so we can study the quench of the superconductors.

The case of temper simulates heat propagation and simulations related to temperature. For this thesis, we mainly used the Magnet, a module that simulates the Maxwell equations in the \boldsymbol{H} formulation. Hence we will go for a more extended explanation below.

3.4 Magnet module

The magnet module is a module from Alya focused on solving electromagnetic problems. Concretely the module uses the H-formulation explained in section 2.5. This module solves the Magnetic field \boldsymbol{H} using the Finite Element Method, concretely it uses Edge Elements instead of Nodal Elements. The main characteristic of the base functions associated with the edge elements is that the tangential component of the vectorial field (in this case \boldsymbol{H}) is continuous in all the domain. Now we will go through the input data files, some of them are for general usage so any module needs these input files to get started. After we will present the input files specific to the magnet module:

- simulation.dat: This file contains the general data for the execution, for example, the modules, the services, and the time of the simulation
- simulation.dom.dat: the dom.dat file contains the mesh description of the domain such as the boundary conditions, the dimensions, and the geometry.
- simulation.ker.dat: Finally this file has the input data for the Kermod. The Kermod is a module mandatory for all executions. It is also responsible for some extra tools such as the mesh refining tool that allows increasing the definition of the whole mesh by adding divisions to the mesh, with this we have a simple and accessible tool able to turn coarse meshes into more refined ones by changing only a parameter in the same input files of Alya.

3.4.1 Magnet input files

For the magnet module we have the specific input file for the magnetic information regarding the simulation which is named as simulation.mag.dat. This file is the main file for the magnet module, and has many subparts relevant for the understanding of this thesis; it is responsible for the properties of all the materials defined, the output variables or the linear solver parameters. We will do an in-depth explanation about it:

• Material Properties:

The very first part is responsible for the properties of the materials. We have the list of materials and for each of them the main electromagnetic properties, such as the Resistivity, Current, Critical Current or material Permeability.

```
PROPERTIES

MATERIAL 1

Reszz POWER

Jcrzz CONST

Ecrzz 0.0001

ncrzz 30.0

Jc0zz 9.5493d7

murxx 1.0

muryy 1.0

rhozz 1.0

END_MATERIAL
```

```
MATERIAL 4
Reszz POWER
Jcrzz CONST
Ecrzz 0.0001
ncrzz 30.0
Jc0zz 9.5493d7
murxx 1.0
muryy 1.0
rhozz 1.0
END_MATERIAL
END_PROPERTIES
```

Listing 3.1: Material input code

As can be seen in Listing 3.1 we can specify each component of every physical property. Also for the current Jcr we can choose between CONST for a constant value of critical current inputted in JcO or for a special value by choosing USERD. Furthermore, for the calculation of the resistivity, we can choose between CONST similarly to the current input in rho or we can use a power law as in equation 2.5.7 taking into account its dependance on the current. In this case, we need to put POWER in the resistivity variable (Res) and fill the parameters of the expression ncr, JcO, Ecr.

• Numerical Treatment of the Simulation:

The numerical treatment of the simulation is also set here. In this part of the script we can decide all the parameters for the time step, tolerances and also select the algebraic solver for the system of equations.

```
NUMERICAL TREATMENT
  DTMIN
             5.0e - 8
  DTMAX
             1.0e-4
  THETA
             1.0
  NLTOL
             1.0e-4
  NLITE
             15
  NLIDE
  GSLIN
             4
  GSTRI
             4
             4
  GSQUA
  GSTET
             4
  GSHEX
             3
  BDFOR
  STRUC
             Off
  ALGEBRAIC_SOLVER
    SOLVER:
               CG
    CONVERGENCE:
                   ITERA=10000, TOLER=1.0e-6
    PRECONDITIONER: DIAGONAL
     OPTION:
                           ZERO_FIXITY
 END_ALGEBRAIC_SOLVER
END_NUMERICAL_TREATMENT
```

Listing 3.2: Numerical treatment code

In this part of code (Listing 3.2) we define the dtmin and dtmax which limit the range where the timestep dt will be such that dtmin< dt <dtmax. NLTOL defines the tolerance

needed in order to finish a non-linear step satisfactorily.

Lastly there are the ALGEBRAIC_SOLVER options where you can choose the solver used for the final matrix form. For the particular case of the Listing 3.2 CG is the Conjugate Gradient Method. The solver also has its own parameters like the maximum iterations or tolerance ITERA, TOLER and the preconditioner used. In this thesis we use the diagonal of the matrix. This preconditioner shows poor performance in some of the simulations discussed in chapter 4. There might be the posibility to upgrade the preconditioner as mentioned in 5.2.2.

• Boundary Conditions:

The boundary conditions are also set in this small input file where you can specify the boundary conditions for each boundary in the domain. In our case, we have Dirichlet Boundary Conditions, codified with the number 2. Neumann Boundary Conditions are not available for the magnet module.

• Output and Post processing:

Apart from running the simulation, Alya should output some time steps so we can analyze the numerical results. However, sometimes the amount of time steps is very large hence saving all the data will result in large amounts of data.

This part of the script is dedicated to tuning the output variables and with which frequency in time steps do we want them, for example, if the simulation has 1000 time steps we can tune it in order to get output files every 100 steps, with this we would only have 10 output files instead of 1000.

```
OUTPUT&POSTPROCESS
  START_POSTPROCESS_AT
                        STEP=0
  POSTPROCESS MAGNE, STEPS=100
  POSTPROCESS CURCZ.
                     STEPS=100
  POSTPROCESS CURNZ, STEPS=100
 POSTPROCESS MAGCE, STEPS=100
  POSTPROCESS FLUXN, STEPS=100
 POSTPROCESS FLUXC, STEPS=100
 POSTPROCESS FORCN, STEPS=100
 POSTPROCESS FORCE, STEPS=100
  POSTPROCESS JOULN, STEPS=100
 POSTPROCESS JOULC, STEPS=100
 NRJOUTPUT On
 MTZOUTPUT On
 VLMOUTPUT Off
 CRNOUTPUT Off
END_OUTPUT&_POST_PROCESS
```

The script allows you to decide at which time step will start the saving of variables in the START_POSTPROCESS_AT. In this case we start the count at the very first step. The variables that are calculated in these simulations can be grouped in pairs. The nodal value of the variable with an N and a smoothed value with a capital C. This module has as outputs the magnetic field MAGNE, MAGCE, the current as CURCZ, CURNZ, the magnetic flux as FLUXN, FLUXC, the force with FORCE, FORCN and finally the dissipated energy JOULN, JOULC.

Apart from these domain variables, there are other global outputs, for example, the integral of all the energy dissipated at each time step NRJOUTPUT. For the script above we will have as output a data file of each domain variable every 100 steps and two extra files for the integral of the energy dissipated and the mtz at each time step which is a parameter still in development trying to get the magnetization of the domain.

• Miscellaneous Options (self-field, edge elements, etc) Finally, we have some options specific for this module such as the self-field option and the edge element option.



The SELF_FIELD option activates the Biot-Savart calculation for the material requested. This allows the domain to have less air because the field on the boundary is calculated with the Biot-Savart law detailed in 2.5.8. In this particular case, it is only calculated for the material 1.

The drawback is that despite the fact that you can reduce the air with this option, for each nodal or edge calculation the Biot-Savart law needs to be calculated by going through all the other points. This can be highly costly in terms of computation. Further to this, we have the EDGE_ELEMENTS option that enables the edge element calculation instead of nodal element calculation. This option is very important for the \boldsymbol{H} formulation as explained in the last paragraph of subsection 3.1.1.

A general overview of all the parameters can be done in order to summarize all the input parameters needed for running these simulations (in table 3.1).

Table 3.1: Summary of the parameters in the magnet module with the section in the code (Subscript) and a brief description.

| Input Parameter | Subscript | Brief Description |
|-----------------|------------|---|
| Reszz | PROPERTIES | Type of resistivity for the material, CONST for a constant value and POWER for the power law |
| Jcrzz | PROPERTIES | Type of critical current, CONST for a constant value USERD for the option in MOD_MAT_MATPRO.f90 |
| Ecrzz | PROPERTIES | The E_c value of the power law for resistivity |
| ncrzz | PROPERTIES | The n value of the power law for resistivity |
| Jc0zz | PROPERTIES | The constant current if Jcr is CONST |
| murxx, muryy | PROPERTIES | Value of μ_r for each spatial direction |

| rhozz | PROPERTIES | Value for the resistivity if Res is chosen as CONST |
|-------------------|-----------------------|---|
| SELF_FIELD | PHYSICAL_PROBLEM | On/Off for applying the Biot-Savart law for a determined material |
| edge_elements | PHYSICAL_PROBLEM | On/Off for using Edge Elements instead of Nodal Elements |
| DTMIN/DTMAX | NUMERICAL_TREATMENT | Minimum and maximum timestep for the solver |
| NLTOL | NUMERICAL_TREATMENT | Tolerance of the non-solver to accept that a step has converged |
| SOLVER | ALGEBRAIC_SOLVER | Algebraic solver, in this case CG (Conjugate Gradient) |
| convergence\ITERA | ALGEBRAIC_SOLVER | Maximum number of iteration for the iterative linear solver |
| convergence\TOLER | ALGEBRAIC_SOLVER | Tolerance of the algebraic solver in order to accept a solution |
| preconditioner | ALGEBRAIC_SOLVER | Preconditioner used for the algebraic solver, in this case DIAGONAL which is the diagonal of the matrix |
| postproc MAGNE | OUTPUT_&_POST_PROCESS | Outputting the Magnetic Field Strength \boldsymbol{H} at the nodes by projecting the solution from the quadrature nodes |
| postproc CURCZ | OUTPUT_&_POST_PROCESS | Outputting the z-direction Current at the element averaging from the Gauss nodes |
| postproc CURNZ | OUTPUT_&_POST_PROCESS | Outputting the z-direction Current at the nodes by projecting the solution from the quadrature nodes |
| postproc MAGCE | OUTPUT_&_POST_PROCESS | Outputting the Magnetic Field Strenght \boldsymbol{H} at the element averaging from the Gauss nodes |
| postproc FLUXN | OUTPUT_&_POST_PROCESS | Outputting the Magnetic Flux density \boldsymbol{B} at the nodes by projecting the solution from the quadrature nodes |
| postproc FLUXC | OUTPUT_&_POST_PROCESS | Outputting the Magnetic Flux density \boldsymbol{B} at the element averaging from the Gauss nodes |
| postproc JOULN | OUTPUT_&_POST_PROCESS | Outputting the Magnetic Field at the nodes by projecting the solution from the quadrature nodes |
| postproc JOULC | OUTPUT_&_POST_PROCESS | Outputting the Dissipated Energy at the element averaging from Gauss nodes |

| NRJOUTPUT | OUTPUT_&_POST_PROCESS | Outputting an archive magnet.nrj with all the time steps and the integral of the energy dissipated |
|---------------------|-----------------------|--|
| BOUNDARY_CONDITIONS | BOUNDARY_CONDITIONS | Choosing of boundaries and their boundary conditions. |

Other files 3.4.2

With these input files together with the mesh files we have most of the information in order to run the simulation. However there is some information that remains inside Alva code, such as the boundary conditions or the Current distribution when putting the Jcr variable in USERD mode.

These folders are kept in the path Alya\Sources\Modules\magnet\; in here we have all the subroutines regarding the specific magnet module. Mainly we will focus in two files:

• MOD_MAG_INPDAT.f90: It contains all information regarding the boundary conditions, the initial field and the external field at each time step. In this file we will code the concrete case of our interest as follows:

$$\mathbf{H}_0 = (0, 0.5, 0) \ T \tag{3.4.1}$$

$$\mathbf{H}_{0} = (0, 0.5, 0) T$$

$$\begin{cases}
\mathbf{H}(t) = 0.5 \cdot \cos(100\pi \cdot t) \cdot (0\mathbf{i}, \mathbf{j}, 0\mathbf{k}) T & t \in [0, 0.005] \\
\mathbf{H}(t) = 0 T & \text{otherwise}
\end{cases}$$
(3.4.1)

Note that equation 3.4.1 and equation 3.4.2 coincide at t=0 in order to keep continuity for the problem the initial conditions and the boundary conditions have to be consistent. For a more extended description on how this is implemented in the file see Appendix A

• MOD_MAG_MATPRO.f90: This other file contains the information regarding the variable current distribution. In here we put the small script calculating the expression of equation 4.2.5. The full code of this implementation can be read on the Appendix

These files are similar to the ones to the previous section except for the fact that they are stored in the same Alya's code. This causes that the code needs to be compiled every time one changes something in these files.

This is because these files are actually not input files but Alya's general files. Further work could be to change these inputs from Alya general files to real input files. In order to compile Alya you need to go to the root directory of Alya and afterwards follow the path alya\Executables\unix and in there run the command make. This will compile again all the Alya code that has been changed.

3.5 Simulation Guidelines

In 1.2 we saw the steps followed in this thesis to obtain satisfactory results. In this section we will have a more detailed description of these steps regarding the preprocessing, simulations and post-processing.

There will be three main steps to follow: the first regarding the preprocessing issues, the second focused on the simulation setup and finally the third concerning the post-processing and visualization.

3.5.1 Problem Preprocessing and Setup

To run a simulation using an HPC FEM (Finite Element Method) code such as Alya, the first task needed is to build the mesh where the problem is going to be solved.

This step is done with the external software Gmsh, an open-source meshing software able to mesh simple geometries. From the documentation, if needed it can be used to mesh more complicated meshes but requires of more advanced level on this software. The complexity of the domain used here was simple enough. The meshing could be done with domains such as circumferences, spheres, regular polygons, or parallelepipeds; this together with extrusions everything could be done.

When the problems got bigger and the mesh gained importance some more advanced tools were used such as the type of elements in the mesh and progressions on the size of the elements (in an axis put elements larger on one extreme and smaller on the other progressively). After this, the mesh has to be post-processed to be read by Alya. This could be done with an existing program which uses the output mesh from *Gmsh* and extra data archives to build the mesh in the format Alya can read it.

Finally, the mesh is uploaded in *Marenostrum 4* and the setup of the problem needs to be done by putting the desired options and values in Alya's input archives simulation.mag.dat but this is more detailed in chapter 3. Also depending on the problem the initial conditions or Current conditions have to be changed in some archives within the same Alya code mod_mag_inpdat.f90 for the boundary conditions and mod_mag_matpro.f90 for the Current conditions.

3.5.2 Simulation of the Problem and Model Debugging

When it comes to the simulation, launching a shell code is needed to put the simulation in the $Marenostrum\ 4$ queues, here is the point where the number of cores and the simulation time has to be set. If the time is below the 2:00h and the cores do not exceed the number of cores in 16 nodes (corresponding to 768 cores)¹ the simulation can be queued in the debug queue and the resources will be given quite fast; if not, the simulation will be queued in

¹For further information about the characteristics of Marenostrum see https://www.bsc.es/support/MareNostrum4-ug.pdf

the main queue where the waiting time for the simulation to start can be from minutes to several hours.

Once the simulation has finished some main archives must be checked to see if in general Alya could finish the simulation or if it had any fatal error or convergence problems. For this the shell code for the simulation keeps two archives, the simulation.out for all the terminal outputs that the simulation has done and simulation.err for the terminal error outputs. When this is checked and looks good we can proceed to the post-processing

3.5.3 Post-processing and Data Visualization

Finally, when the simulation has ended and the check has been made we can proceed to the data post-processing. Alya outputs some time steps that can be interesting for the visualization but in a format that cannot be read by most post-processing tools. Fortunately, Alya includes a small software to post-process this data to readable outputs. This software is called Alya2pos and as it says, converts the Alya archives to position and data on each point. This same tool can be used in the same *Marenostrum 4* because sometimes the amount of data to post-process can be too much for an ordinary computer.

After this, the data is exported from *Marenostrum* 4 to the personal computer where the data can be read with another external open-source software called *Paraview*. Again it is similar to *Gmsh*, the level of usage of these tools for the thesis has been quite basic but they have much more utilities. In particular, Paraview can work in parallel using different cores of the computer and can get many types of plots and data outputs.

In our case, we did not need to use many tools. Only the typical vector or potential plots over surfaces as well as slicing the domain to see inner parts or plotting determined variables over a concrete line. This last tool has been quite useful because you can save the plotting data in a .csv so by plotting the Magnetic Field at $400\mu m$ from the surface of the tape and saving the .csv we could extract the array of data to be compared directly to the ICMAB experimental results. Other auxiliary Python codes have been written and used to post-process or compare output data from Paraview and ICMAB data.

Chapter 4

Results

After the introduction to Superconductivity and the Alya code, in this chapter we will present the experiment carried out by ICMAB. Which we will use as a first test case for our experimental validation of the magnet module.

Thereafter we will go through the simulations performed. Simulation results are ordered from the simplest case to the most complex case. Each section presents a different simulation setup and compares it with the experiment. The goal is to identify which setup gives the closest results to the experimental data from ICMAB.

4.1 Modelling ICMAB experiment

ICMAB *Institut de Ciencia de Materials de Barcelona* is an Institute focused on the research of new materials, some of them superconductors. The experiments modelled in this work have been carried out by Dr. Xavier Granados and Neil Lamas.

The general setup of the experiment was to place a superconducting tape of size ($12 \text{ mm} \times 50 \,\mu\text{m} \times 12 \,\text{cm}$) from the company THEVA in a cooling system (turned off at the beginning). The tape is placed along the z-axis and a magnetic field $B_y = 0.5 \,T$ was applied. After this, the superconductor was brought to the superconducting state by cooling it to 77K.

The order of the steps is relevant because adding the magnetic field firstly allows the field lines to penetrate the material. Afterwards, cooling it down brings the material to the superconducting state without expelling the magnetic field. If this was done on the other way round (first cooling and then applying the magnetic field) the superconductor would compensate the field applied by generating current loops due to Faraday's Law.

It is important to note that here we do not consider the Meissner-Ochsenfeld effect. This is because the HTS tape used is a Type-II superconductor and the regime of the superconductor we are working on is the mixed state or region between H_{c1} and H_{c2} ; in this regime, as we said in previous chapters, we do not have a complete Meissner-Ochsenfeld Effect and so the material will not expel the magnetic field but will pin it in magnetic vortices.

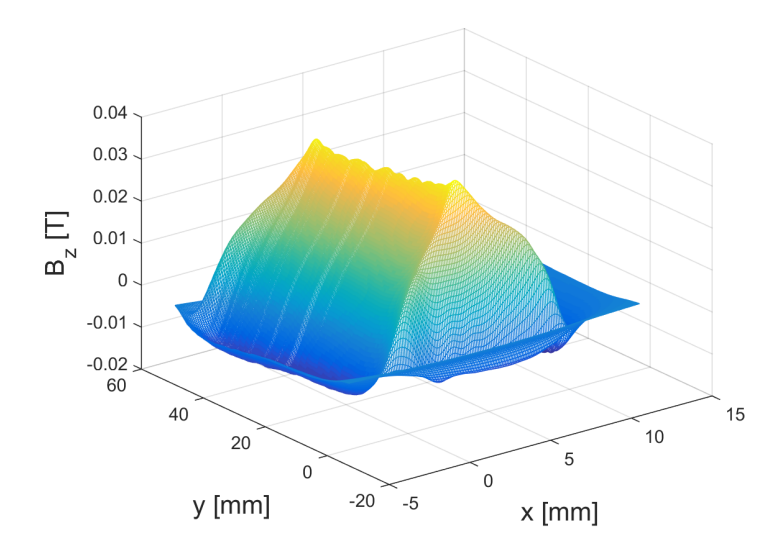


Figure 4.1: Mapping of B_z measurements from ICMAB (courtesy of Neil Lamas, ICMAB)

With this situation, the initial magnetic field is decreased and, due to Faraday's Law, the superconductor will create currents opposing to this variation of the magnetic field. Once the field is carried to $B_y = 0$ T the superconductor would have created a whole current distribution according to the Critical Current Density of the material trying to compensate for the variation of the magnetic field.

In ICMAB experiments the permanent field created by the current loops was measured after a relaxation time of the order of minutes. The field is evaluated on the Y direction with a device that measures it through the Hall Effect at 400 μm . With this, they managed to get a 3D surface where the X and Y were the spatial coordinates and Z is the magnetic field B_y measured at each pair (x, y) given that the z coordinate is fixed to 400 μm from the surface of the tape.

We have to note that ICMAB used the axis differently, in our case we placed the tape on the X-Z plane and measured the field on the Y axis, whereas in their case (see figure 4.1) they placed the tape on the X-Y plane and measured the field on the z-axis. Another fact is that despite the tape is 12mm long they measured the central part to avoid distortions caused by boundary effects.

4.1.1 Considerations for the modelling

A couple of considerations are needed in order to move from this real problem to the simulation.

First of all, knowing that the tape has a very thin layer of superconductor covered with several layers of copper, Hastelloy, or even buffer layers (see figure 4.2), we will considerate that we work with a thicker homogeneous superconductor tape of $w=100~\mu m$. This assumption is feasible because once we know the Critical Current Density of the real tape, we can extrapolate the new Critical Current Density by calculating the total current that can flow in the original tape. Thus, we can define its flow as the total current.

Moreover, magnet from Alya uses the Finite Element Method for the \boldsymbol{H} formulation as well as the Power Law for the resistivity. This works very well for actively changing fields but not for relaxation. The experiment at ICMAB was brought from 0.5T to 0 and afterwards, they waited several minutes before taking measurements. In our case, knowing that the power-law dissipates slowly the currents in relaxations problems when theoretically superconductors do not dissipate currents, we will just have a millisecond of relaxation. According to this, we shorten the computation time while avoiding problems with the dissipation of energy during this period.

TPL4000 series: Surround Copper stabilization for all kinds of applications. Copper surround coating electrical + mechanical stabilization -Silver surround coating contact laver -HTS layer - high performance functional layer -Second MgO buffer layer optimized for HTS layer growth -First MgO buffer layer - textured by inclined Hastelloy® C-276 substrate substrate deposition -- non magnetic, high strength

Figure 4.2: Scheme of the THEVA tape (obtained from THEVA [accessed: February 9, 2022])

4.2 2D Simulations

For the 2D simulation we based our work on the fact that the tape and the results expected will have symmetry in the z direction if the tape is long enough. Our first mesh is presented in figure 4.3

In this mesh we used a section of the tape with size $(1 \times 120) \cdot 10^{-4} \ m$, the total domain-containing air is a circumference of radius $R = 80 \cdot 10^{-4} \ m$. We used triangles to mesh the domain and we achieved a number of edges $\# = 33062^{1}$ and a total of 80 boundary edges.

In the first 2D simulation we set an initial magnetic field of $B_y = 0.5 T$. The external magnetic field decrease was defined with the following expression:

$$\boldsymbol{B} = 0.5 \cdot \cos(100\pi \cdot t) \cdot (0\boldsymbol{i}, \boldsymbol{j}) \tag{4.2.1}$$

¹Note that we showed edges instead of node because magnet uses edge-element FEM

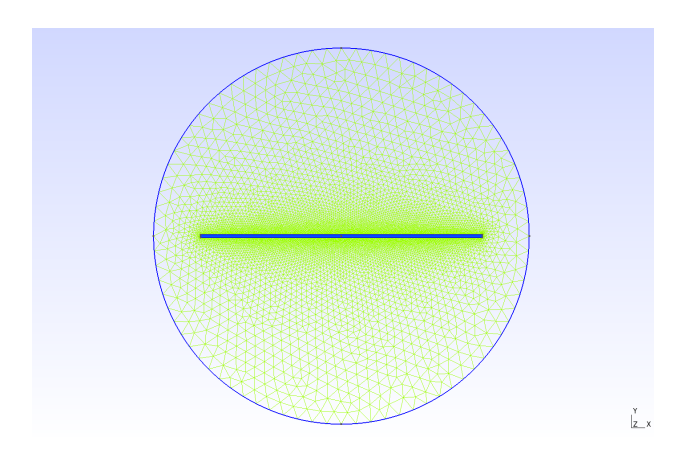


Figure 4.3: 2D first mesh done with Gmsh

This is the expression of a magnetic field on the Y direction decreasing as a cosine of frequency $f = 50 \, Hz$ so we put a simulation time between $0 - 6 \, ms$ where from 0 to 5 ms the field decreases from 0.5 T to 0 T according to eq. (4.2.1). Afterwards, the field condition is set to 0 T in order to let some relaxation time.

4.2.1 2D simulation with Self-Field

Another important issue to bear in mind is that we will use from the beginning the Self Field option for the Superconductor. This option considers the Biot-Savart Law (see subsection 2.5.2) to calculate the magnetic field at one point. This configuration allows a smaller air domain and consequently, a smaller number of nodes.

| Edges | Boundaries | Total space | Cores | Elapsed time |
|-------|------------|-----------------------------|-------|--------------|
| 33062 | 80 | $2.01 \times 10^{-4} \ m^3$ | 48 | 2:52h |

Table 4.1: Summary of the setup and performance of the 2D with Self-Field

With this number of edges, a total number of 48 cores were used to perform the simulation. From now on, all the outputs from each simulation will be summarised in a table to be able to compare simulations between them.

As seen in table 4.1 the elapsed time is 2:52h, a value larger than 2h which means that the normal queue has been used for this simulation. This means that the total time from launching the simulation until getting the results has been substantially longer than this 2:52h.

From figure 4.4a we observe the current on the left-hand side pointing outwards and the current on the right-hand side pointing inwards. This shows that the superconducting tape has generated a current loop to compensate for the external field variation. This case shows a 2D current distribution instead of surface currents which will be expected for a perfect superconductor. This is because of the Finite Critical Current of the tape.

Another approach for the current density can be to plot the current distribution at the

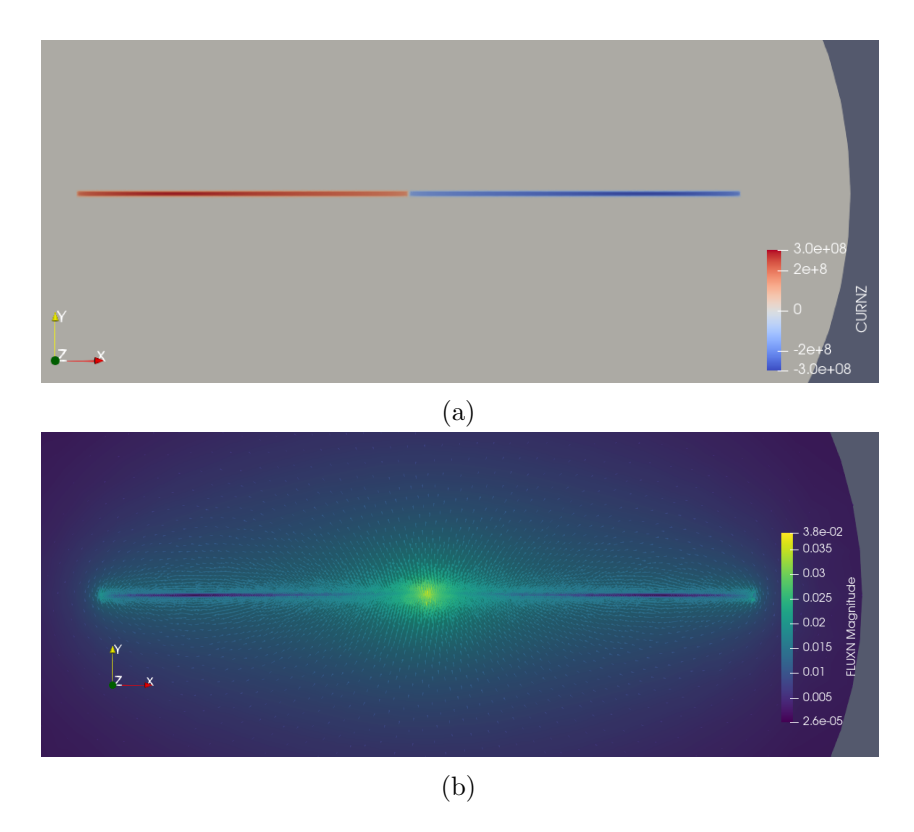


Figure 4.4: (a) Plot of the Z component of the Current (A) and (b) Magnetic field generated by the superconductor tape (T)

center of the tape (see figure 4.5) the results achieved show this antisymmetric behavior of the current loop.

Figure 4.4b shows the \boldsymbol{B} field created by the current distribution. The value plotted is the magnitude of the magnetic field. In the center the field is pointing upwards and at the borders it is pointing downwards trying to compensate for the removal of the 0.5 T field it had at the beginning.

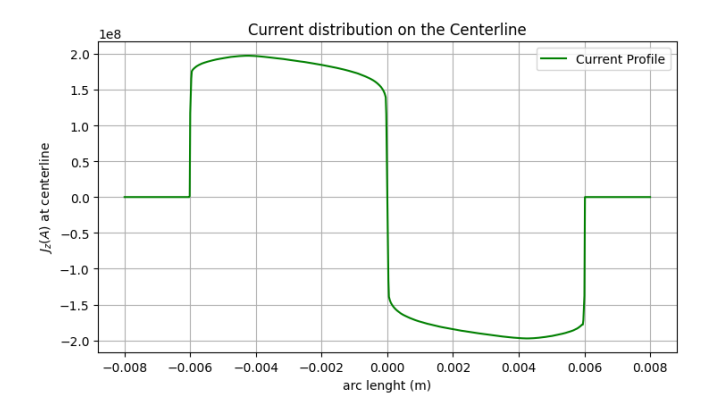


Figure 4.5: Current distribution from a tape with constant J_c

In order to check if the magnet module reproduces well the superconductivity phenomena we have compared it with the data measured in *ICMAB*. In figure 4.6 we notice a good agreement between the simulated results and the experimental ones, the main difference emerge when comparing the simulated symmetric profiles against the experimental asymmetric shape in some parts.

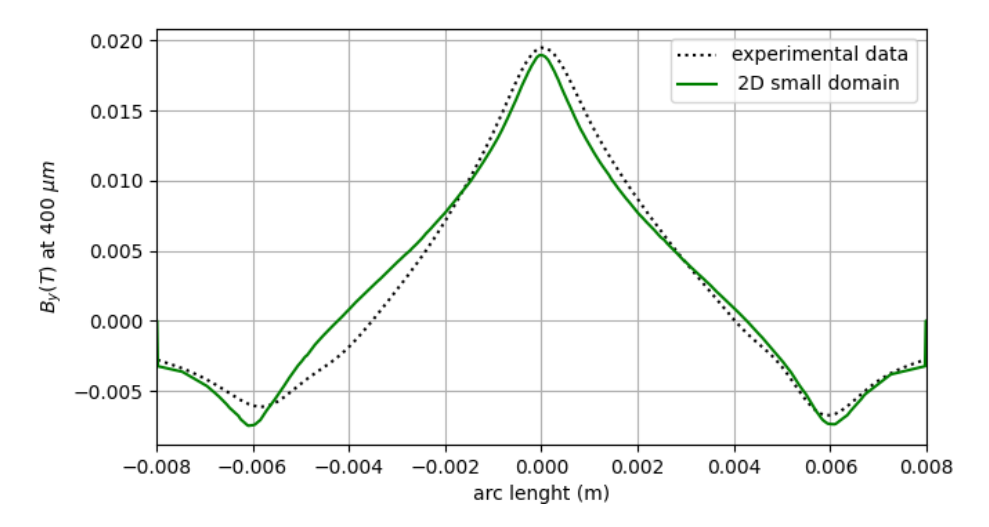


Figure 4.6: B_y field at $400\mu m$ of the tape for the small 2D domain, the tape goes from -0.006-0.006 m according to the tape width of 12 mm

It is important to point out that the simulation took longer than expected when the field got close to zero. This was due to the time step taken, when the convergence of the problem is not sufficiently good Alya repeats the step with a smaller time step. In this case, we observed how it went to time steps $dt \sim 10^{-10}s$.

This reveals Alya is having problems with solving properly the problem and that it needs at times very short time steps to keep the convergence. This problem may come from the *Self Field* option which is calculating the Biot Savart Law for all the points in the Superconductor. This option is still not fully developed and optimised so it may cause some troubles. For further simulations, we will deactivate this option in order to achieve better performance results.

4.2.2 2D Simulations without Self-Field

Principally, the Self-Field option is used to reduce the air domain and in consequence the total domain and the number of nodes. The Self-Field or Biot-Savart option is useful for small domains or cases where fields remain finite. For large domains it slows down the calculations because of the complexity of the process. In particular, to obtain the magnetic field it is needed to go through all the edges in order to get the value for the integral 2.5.8.

To avoid convergence problems we try to simulate the same problem as in the previous section but deactivating the self-field. With this we will keep the proper convergence in the $\mathbf{B}=0$ T time steps.

However, after launching the simulation we observe how Alya has even more problems to converge, which is something we have not came across before. Here we have a piece of the code in which we can observe how it is unable to do even a single step. The solver can compute many steps but the error is not reduced enough to consider that the step has converged. We hypothesize that this is caused by the lack of air domain when removing the Self Field option. With the Self Field the problem could converge with less air but removing the option causes convergence problems until the air is increased.

```
ALYA
           RESTARTING TIME STEP 3
                    680
                              Res. =
                                       0.9844E-10 \text{ gloRes} = 0.8771E-07
                                                                              relRes
  1. ls Iter. =
                           1s
                              0.6409E-02
                                                      0.5081E+08
     0.4378E-01
                                            Hnorm =
                   solVar
                   3694
                           1s
                                       0.9597E-10
                                                                              relRes
     ls Iter. =
                                                    gloRes =
                                                                0.3853E-03
     0.1923E+03
                   solVar =
                              0.3313E-05
                                            Hnorm =
                                                      0.5081E+08
                                                     gloRes = 0.1393E-03
  3.
     ls Iter. =
                   3515
                           ls
                              Res. =
                                       0.9591E-10
                                                                              relRes
     0.6955E+02
                   solVar
                              0.3198E-05
                                            Hnorm =
                                                      0.5081E+08
                                       0.9895E-10
  4.
     ls Iter. =
                   3769
                           ls
                              Res. =
                                                     gloRes = 0.5039E-04
                                                                              relRes
     0.2515E+02
                   solVar =
                              0.3089E-05
                                            Hnorm = 0.5081E + 08
                                                     \overline{\text{gloRes}} = 0.1822E - 04
                   3891
                                       0.9623E-10
                                                                              relRes
  5.
     ls Iter. =
                           ls
                              Res. =
     0.9097E+01
                   solVar =
                              0.2988E-05
                                            Hnorm =
                                                      0.5081E+08
     ls Iter. =
                   3968
                           ls
                              Res. =
                                       0.9939E-10 \text{ gloRes} = 0.6591E-05
                                                                              relRes
     0.3290E+01
                   solVar =
                              0.2889E-05
                                            Hnorm =
                                                      0.5081E + 08
     ls le r. =
                   4027
                           ls
                              Res. =
                                       0.8669E-10 \quad \text{gloRes} = 0.2384E-05
                                                                              relRes
     0.1190E+01
                              0.2793E-05
                   solVar =
                                            Hnorm =
                                                      0.5081E+08
                                       0.9919E-10 \text{ gloRes} = 0.8621E-06
  8.
     ls Iter. =
                   3996
                           1s
                              Res. =
                                                                              relRes
     0.4303E+00
                   solVar =
                              0.2700E-05
                                            Hnorm =
                                                      0.5081E+08
                              \underline{\mathrm{Res.}} = 0.9672 \underline{\mathrm{E}} - 10 \quad \underline{\mathrm{gloRes}} = 0.311 \overline{\mathrm{8E}} - 06
                   3648
                                                                              relRes
  9.
     ls Iter. =
                           1s
     0.1556E+00
                              0.2610E-05
                                                      0.5081E + 08
                   solVar =
                                            Hnorm =
                   3404
                                       0.9769E-10
                                                    gloRes = 0.1128E-06
                                                                              relRes
 10.
     ls Iter. =
                           1s
                              Res. =
     0.5629E-01
                   solVar =
                              0.2523E-05
                                            Hnorm = 0.5081E + 08
 11.
     ls Iter. =
                   3064
                           ls
                              Res. =
                                       0.9606E-10
                                                     gloRes = 0.4078E-07
                                                                              relRes
     0.2036E-01
                   solVar =
                              0.2439E-05
                                                      0.5081E + 08
                                            Hnorm =
     ls Iter. =
                   2647
                           1s
                              Res. =
                                       0.9858E-10
                                                     gloRes = 0.1475E-07
                                                                              relRes
 12.
     0.7362E-02
                   solVar =
                              0.2357E-05
                                            Hnorm = 0.5081E + 08
    ls Iter. =
                   2169
                              Res. =
                                       0.9873E-10 \text{ gloRes} = 0.5334E-08
                                                                              relRes
 13.
                           ls
     0.2663E-02
                   solVar =
                              0.2278E-05
                                            Hnorm = 0.5081E+08
 14. ls Iter. =
                           1s
                              Res. =
                                       0.9888E-10 \text{ gloRes} = 0.1929E-08
                                                                              relRes
                   1464
     0.9629E-03
                   solVar =
                              0.2201E-05
                                            Hnorm = 0.5081E+08
                              Res. = 0.9812E-10 gloRes = 0.6975E-09
                           ls
 15. ls Iter. =
                   1027
                                                                              relRes
     0.3482E-03
                   solVar =
                              0.2123E-05
                                            Hnorm = 0.5081E+08
Convergence was not reached. Reduced time step will be used, dt = 0.5000E
  -09
 ALYA
        CRITICAL TIME OVERSHOOT
 ALYA
        GOING BACK TO TIME t=
                                   1.625000E-09
            RESTARTING TIME STEP 3
 ALYA
```

In 4.2.2 we saw a typical output of Alya's terminal. We observe how the gloRes is almost not reduced in the same timestep, that is why Alya requires for going back to the previous time step. Concretely it is going back to the third time step which is almost in the beginning.

We entered an endless loop where the timestep size cannot be reduced because of the dtmin=5.0e-10 but even if we reduce the dtmin we would receive similar problems, also we are not interested in very small time steps because the simulation would take a long time to finish. Our strategy will be to increase the air domain substantially to avoid these convergence problems.

4.2.3 Increased Air Domain

In this new setup we used the same GMSH script but increasing the radius of the external circumference from $R=80\times 10^{-4}\,\mathrm{m}$ to $R=50\times 10^{-3}\,\mathrm{m}$ which represents an increase of approximately $\times 40$ of the air domain.

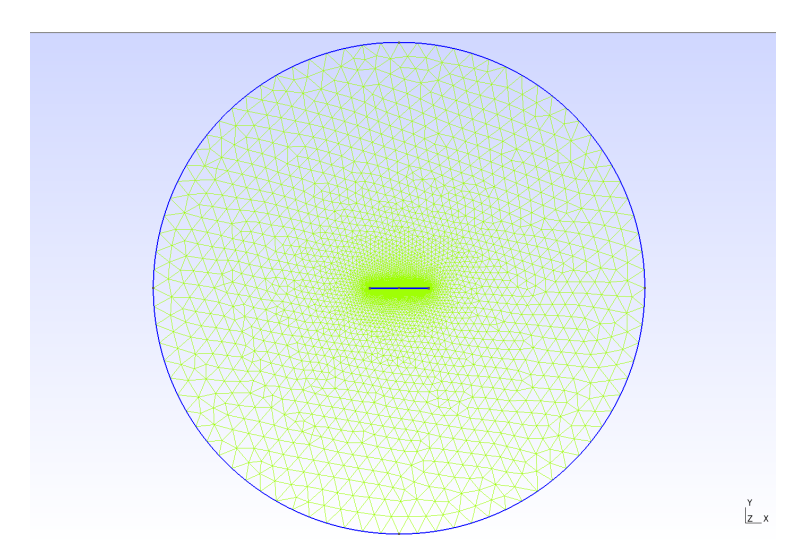


Figure 4.7: 2D increased air domain mesh

The tape remains the same size as in the previous simulation but due to the larger domain and the new meshing the number of edges has increased now to 44640. Furthermore, we remind that the Self Field option is deactivated now. The setup and performance of the experiment are the following:

| Edges | Boundaries | Total space | Cores | Elapsed time |
|-------|------------|-----------------------------|-------|--------------|
| 44640 | 80 | $7.85 \times 10^{-3} \ m^3$ | 60 | 2:38h |

Table 4.2: Summary of the 2D case with larger air domain

By plotting the same cases as in figure 4.4 we expect to have the same outputs.

From these plots, we can only see qualitatively that the results are very similar, but what is really of our interest is if it matches the experimental data obtained by *ICMAB*. Thus, we can get the same plot as in figure 4.6 but adding this new profile and compare the two simulations, one with small domain and Biot Savart, and the other with a larger domain but removing this *Self Field* option; to the experimental data.

From figure 4.9 we observe an excellent agreement between the two simulations, the only small difference is the fact that the new simulation with a larger domain has slightly larger peaks both in the center and in the borders of the tape. Despite these small differences, the general behavior is the same as in the previous case but now without having convergence problems when the field tends to zero.

In conclusion, by removing the Self Field option and adding more air the results match with the previous cases while we achieved to reduce the elapsed time by 20 min. The

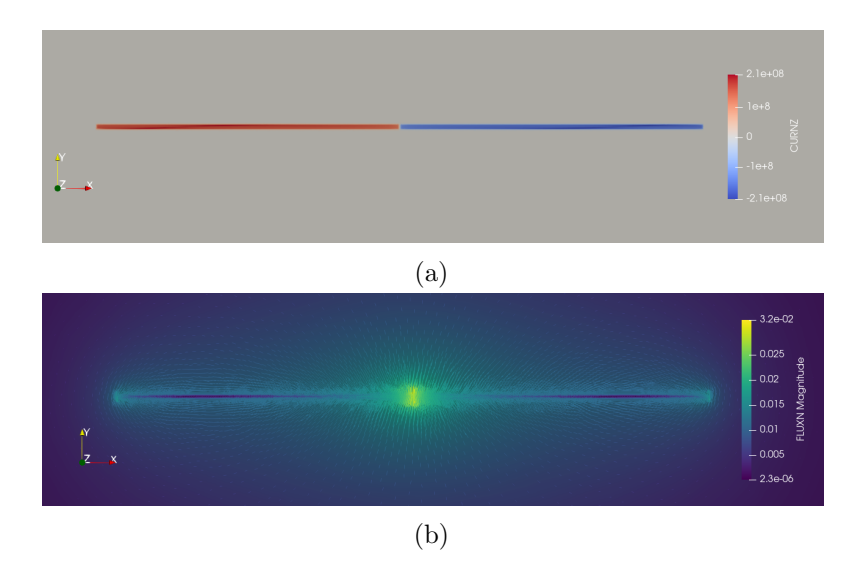


Figure 4.8: (a) Plot of the Z component of the Current and (b) Magnetic field generated by the superconductor tape for the Increased Air Domain experiment

only issue we should try to solve before going to 3D is this asymmetry we observe in the experimental results which are not shown in the simulations. For this, we will next explore a specific feature of the THEVA tapes, that is the angular tilting of the crystalline structure of the tape.

4.2.4 Dependence on Magnetic Field Orientation

Superconducting tapes are highly anisotropic and have different current densities depending on the axis the current is flowing through. THEVA tapes have a small issue regarding the crystal lattice orientation, the c-axis (axis of the crystalline structure) of the lattice is tilted 30° from the normal (see miniature in figure 4.10a). This physical feature can affect directly the current distribution and may be the reason for the asymmetry observed in the ICMAB experimental data.

In order to have a more realistic simulation we will change the homogeneous and independent critical current distribution J_c by a critical current distribution that depends on the magnetic field, both amplitude and direction $J_c(\theta, \mathbf{H})$. Regarding this, the THEVA manufacturer provides information on how the temperature and the angle of the magnetic field affect the lift factor of the tape.

$$\mathcal{L}_f(\boldsymbol{B}, T, \theta) = \frac{I_c(\boldsymbol{B}, T, \theta)}{I_c(77K, \text{self field})}$$
(4.2.2)

The lift factor of the tape is a factor multiplying to the Critical Current that can flow through the tape (see equation 4.2.2) and it is obtained by dividing the Critical Current in some conditions by the Current of the self-field at 77 K. This leads to an expression of the Current Density (equation 4.2.3) which at the same time depends on the magnetic field B, the temperature, and the orientation of B. Hence, in general, we will have a Critical Current depending on the temperature, the magnetic field, and the angle of the magnetic

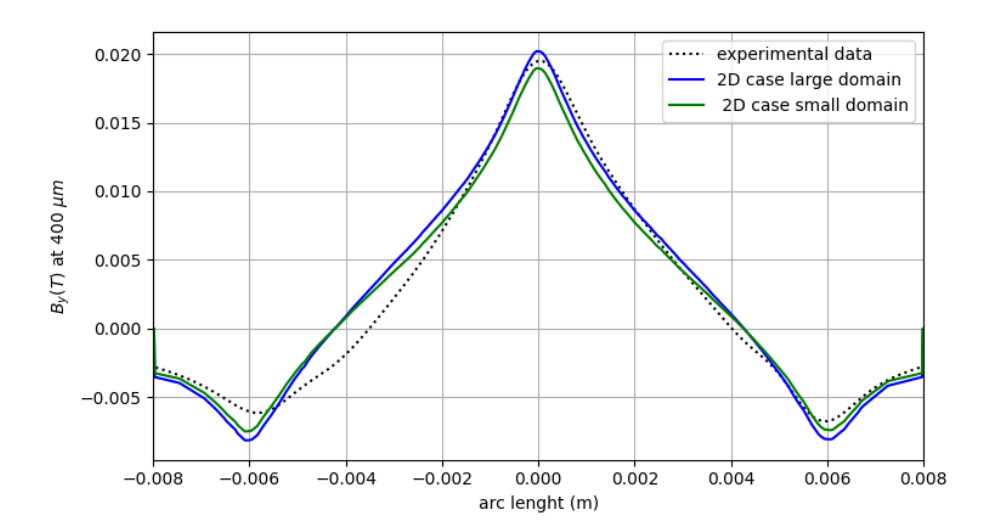


Figure 4.9: Comparison for B_y at $400\mu m$ of the case of the small domain and the new case of the large domain without Self-Field

field rather than a constant value for all the tape. To renormalize the current we divide the Lift factor at certain conditions by the Lift factor at 30° .

$$J_c(\theta, \mathbf{B}, T) = \frac{\mathcal{L}_f(\theta, T)}{\mathcal{L}_f(\theta = \pi/6, T)} \cdot J_c(\mathbf{B})$$
(4.2.3)

In our case, the temperature was fixed to 77K so we only need to focus on the angle and the magnetic field. Out of these two plots we need to get a parametrization that calculates the

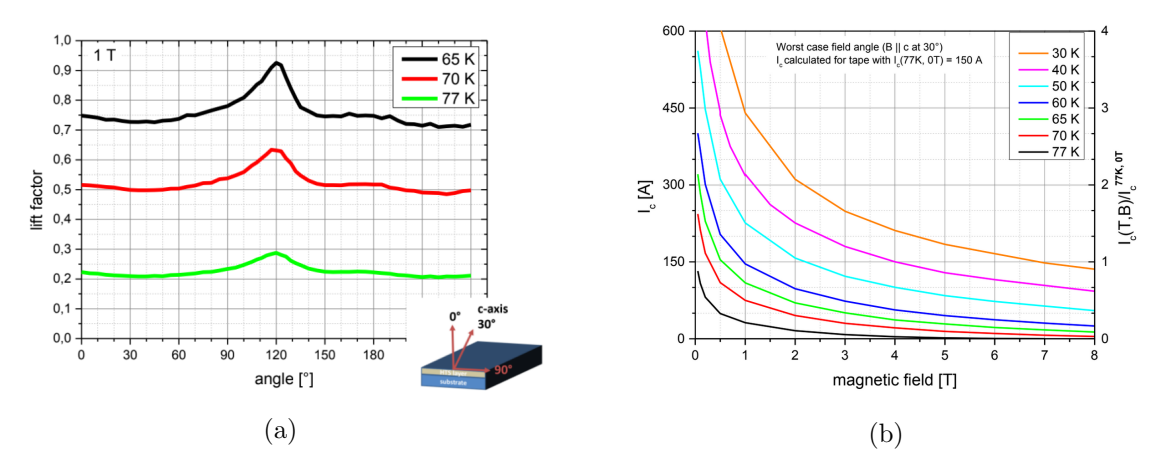


Figure 4.10: (a) Lift Factor for the Current in terms of the angle of the field θ , (b) Critical Current in terms of the magnetic field intensity $|\mathbf{B}|$

Critical Current out of the magnetic field and the angle of the vector field. This has been implemented to Alya through a double parametrization. The first one is done through a fitting on the data given by THEVA in figure 4.10b, which has been done by Neil Lamas in ICMAB.

That fit is the case of the Current in terms of the Magnetic field, the curve at 77K can be represented by the following expression:

$$J_c(\mathbf{H}) = \frac{189.53456}{0.0000012} \left(1 + \frac{|\mathbf{H}|\mu_0}{0.05184} \right)^{-0.50016} \left(1 - \frac{|\mathbf{H}|\mu_0}{7.22788} \right)^2$$
(4.2.4)

Then, we need to multiply this value times the corresponding lift factor of the angle. This will be done through data interpolation. We will include the points of the figure 4.10a in an input file for Alya and now we will calculate the angle of the magnetic field and interpolate the value of the lift factor needed out of the data.

Finally, the expression for the Critical Current or Critical Current Density for each point in the superconductor will be:

$$J_c(\mathbf{H}, \theta) = \frac{\mathcal{L}_F(\theta)}{\mathcal{L}_F(\pi/6)} \cdot J_c(\mathbf{H})$$
 (4.2.5)

Here we multiply by the lift factor \mathcal{L}_F of the angle, but first and foremost we normalize it over the 30 degree value. This is done because the lift factor is a value between 0 and 1 but we want to have as reference the value at 30 degrees ($\mathcal{L}_f = 1$). In a schematic pipeline, what Alya does to calculate this Critical Current Density is:

Inputs
$$\boldsymbol{H}$$
 and (x,y) With \boldsymbol{H} Calculate $J_c(\boldsymbol{H})$ with (H_x,H_y) Interpolate \mathcal{L}_F with θ Use $J_c(\boldsymbol{H}),\mathcal{L}_F(\theta)$ in equation (4.2.5) to obtain $J_c(\boldsymbol{H},\theta)$

This dependence has been included in the file MOD_MAG_MATPRO.f90 and it is explained in more detail in subsection 3.4.2. With this subroutine, we could update the Critical Current density in each point in every timestep according to the local orientation of the magnetic field. Therefore, we can run again the same simulations of the large air domain without the Self-Field option and check which results we obtain.

4.2.5 Results with Angular Dependence

Keeping the same mesh as in figure 4.7, the Self Field option deactivated and now the new option of the variable Current Density we ran a simulation summarised in the following table:

| Edges | Boundaries | Total space | Cores | Elapsed time |
|-------|------------|-----------------------------|-------|--------------|
| 44640 | 80 | $7.85 \times 10^{-3} \ m^3$ | 60 | 5 : 29h |

Table 4.3: Summary of the 2D case with $J_c(\theta, \mathbf{B})$

The summary is quite similar to the previous simulation but a dramatic increase in the elapsed time. This increase arise from the problems Alya had to reach convergence on each step, the general timestep dt is quite smaller than in the previous simulation and often we

reached bottlenecks in the simulation where the timestep had to be reduced even more (close to $dt \sim 10^{-9}s$) to overcome convergence problems.

We can go directly to the plot of the B_y at $400\mu m$ in order to check if the simulation has given good results.

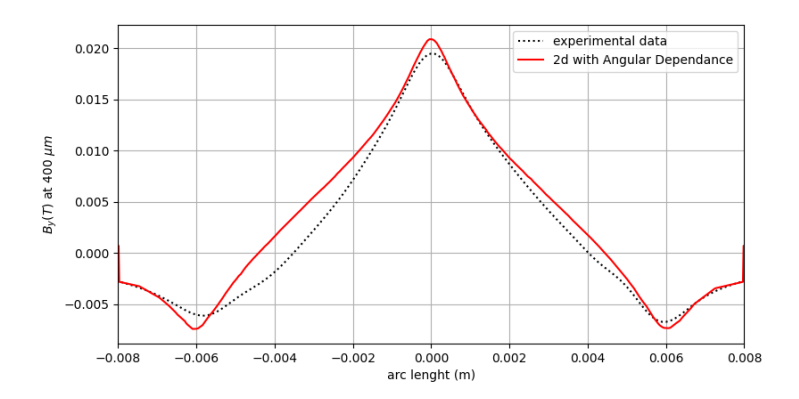


Figure 4.11: B_y profile at 400 μm for the case with $J_c(\theta, \mathbf{B})$

At first sight, and despite the problems with the convergence, the simulation achieved good results (see figure 4.11) although it has not shown any asymmetry as the one we have in the experimental results.

At this point, we could think that either the angular dependence of the Critical Current does not affect enough the magnetic field or that the variable Critical Current depending on the angle and the field is not well implemented. This can be checked by observing the profiles of the current flowing through a few lines at some distance from the center of the tape.

In figure 4.5 we could observe how a constant current density profile looks like: the current rises suddenly when entering the tape and remains close to the value of the Critical Current (In this case 1.9×10^8 A). Also, the two current directions are visible here with this antisymmetric shape.

In general, this is the expected shape of the current distribution on a superconductor with homogeneous Critical Current Density but in our case, and recalling Figure 4.10a, the current should have a peak when the field orientation points to 120° or 300°. Thus, we should expect to have a current distribution non-flat on the tops having a small variation on the Critical Current matching the peak in this small variation with the field pointing to 120°.

To check this we will make a double plot containing both the current distribution and the angle depending on the point for all the lines $\theta(x)$. In this case, the position of the current peak and the position of the angle 120° (according to the peaks in figure 4.10a) must coincide in the space. These small validations need to be done at different distances from the centerline but always in the superconductor because the Current is only flowing inside the tape. From the plots in figure 4.12 we observe that the angular dependent Critical Current is well implemented because it is showing asymmetric peaks on the critical current.

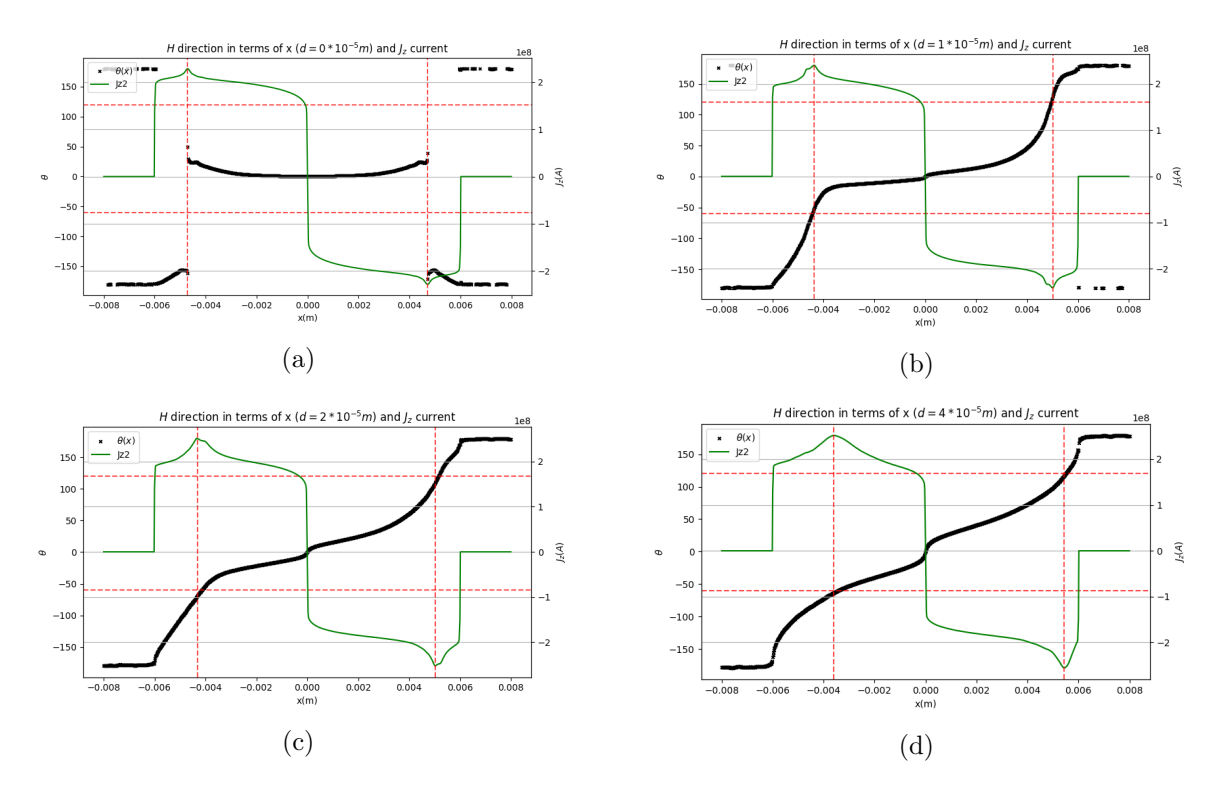


Figure 4.12: Plot of current distribution J(x) and the magnetic field orientation on each position $\theta(x)$ for different distances from centerline in (a) in the centerline, (b) at $10\mu m$, (c) at $20\mu m$ and in (d) at $40\mu m$. In red the lines crossing the angles where the lift factor has its peak and where the current distribution has its peaks.

Concretely, in figure 4.12, it matches the position of the current peak and the position where the angle is 120° or -60° for all the distances in the tape. The only exception is the centerline since the angle will always be 0° or 180° because in this position all the magnetic field lines will point upwards or downwards. Consequently, we will not get any peak on 120° . However, there is a slight peak matching the angle change given that the values of the lift factor at 0° or 180° are not the same.

Therefore, as the angular dependence is well implemented, the only reason to still have the same results on the B_y is that this dependence on the field orientation is not affecting enough the Y component of the magnetic field final profile. This can be checked if we plot the magnetic field separated by components.

In figure 4.13 we can note that despite the current density is presenting these relevant peaks the impact on the magnetic field is secondary. Actually, the largest impact is on the B_x showing asymmetric behavior at the position where the current peak is. However, this effect gets reduced as soon as we move away from the centerline. On the other hand, B_y field seems to remain the same even with the new angular critical current density. This is why we didn't see any substantial change when measuring the B_y at 400 μm . Because of this decrease of the effect with the distance to the centerline the measurements at 400 μm are too far to see any effect of the current peaks. Furthermore, we have been measuring the B_y which seems to have less variation coming from this dependence.

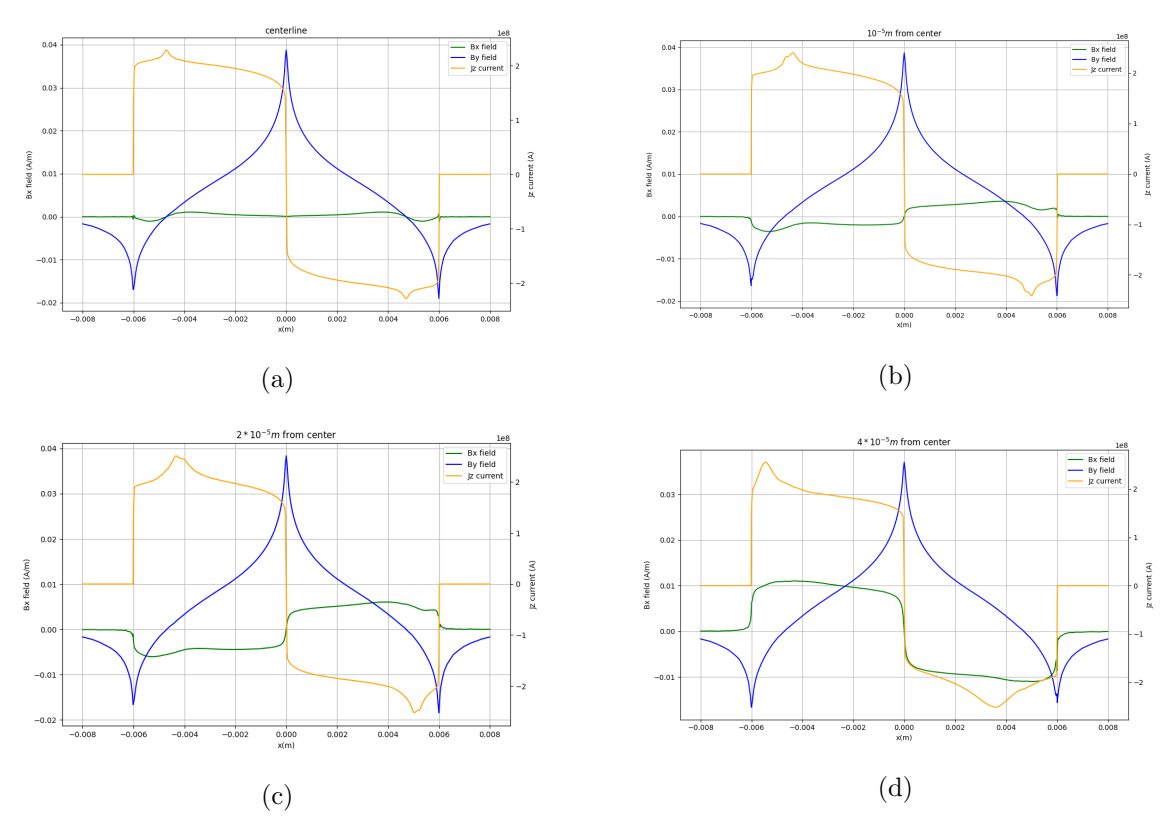


Figure 4.13: Plot of current distribution J(x) and the magnetic field \boldsymbol{B} by components on each position for different distances from centerline in (a) in the centerline, (b) at 10 μm , (c) at 20 μm and in (d) at 40 μm .

We can conclude that we implemented properly the angular Critical Current given by THEVA, and thus we have now a more complete tool to simulate with more detail cases of superconductors. This gives us the chance to include dependencies given either by interpolating data out of tables or by adding an expression depending on other variables. However, we have not managed to reproduce the asymmetry observed by ICMAB with these dependencies even though they caused the simulations to last longer because of extra calculations or convergence problems.

4.3 3D Simulations for the Tape problem

After implementing all the dependencies in the 2D case and having a good agreement with the experimental results we will move forward to the 3D case. We saw that the only drawback of the 2D case is that it was not able to reflect the asymmetry on the magnetic field despite having this angular dependence affecting the critical current.

In this section, we will focus on modelling a 3D experiment and solve it similarly to the 2D case. With it we expect to have a better representation than just a slice of the tape and observe if this 3D case leads to the expected asymmetry.

Just as in the previous section we present the mesh we will be using. In this case we will keep the tape dimensions but adding a length dimension so the final size will be $(1 \text{ mm} \times 12 \text{ mm} \times 12 \text{ cm})$.

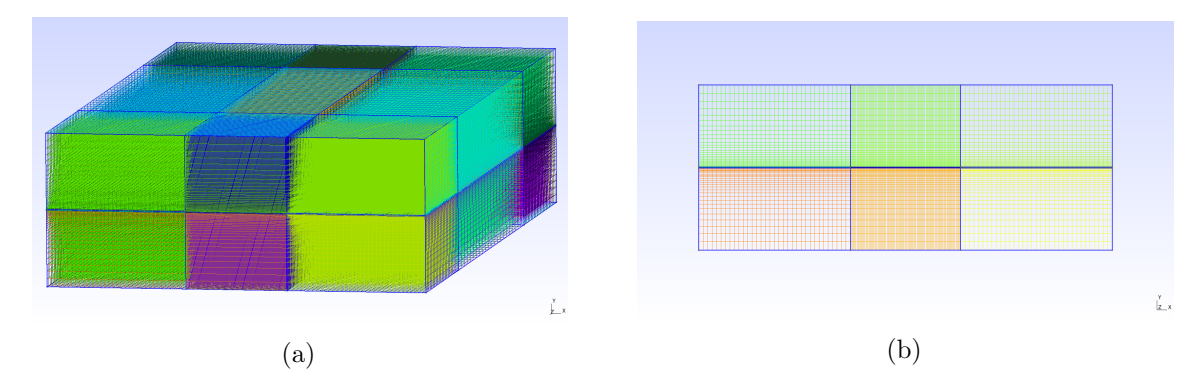


Figure 4.14: (a) 3D mesh in the Gmsh visualization, (b) same mesh viewed from the z direction

In this figure we have the same mesh for the 3D case, in 4.14a we have the 3D visualization and in 4.14b the front view. The colors are just made by Gmsh in order to separate the different regions built. Concretely we have that the tape domain is kept in the inner core of the whole mesh so we only see air domains in these views.

In this situation, the divisions get more relevant because in the 2D case with a quite fine mesh we were using 40000 edges, but for this simulation, keeping a similar number of divisions, we can achieve millions of edges. After some attempts and adding a new tool of GMSH called *progression* we managed to keep the similar sizes of the superconductor and the air elements near the superconductor but progressively increasing the size as we move away from the superconductor.

4.3.1 Tape Length Optimization

With this, we succeeded to reduce substantially the number of edges, but we still need a large number of cores. To reduce the number of cores to allow for a more efficient simulation we focus on the tape length. THEVA tapes used in ICMAB are 12 cm long but as far as we do not have border effects in the central part of the tape, the length can be reduced to a new size where the results will be the same with a lower computational cost.

| Edges Boundaries | Roundarios | Total space | Dimensions of the | Cores | Elapsed | Tape |
|------------------|-------------------------------|------------------------------------|----------------------------|-------|----------|----------------|
| | $(\times 10^{-5} \text{m}^3)$ | domain $(\times 10^{-2} \text{m})$ | Cores | time | length | |
| 1972322 | 49072 | 6.48 | $4.5 \times 1.8 \times 8$ | 584 | 28.6 min | $4\mathrm{cm}$ |
| 3032077 | 65272 | 8.1 | $4.5 \times 1.8 \times 10$ | 896 | 34.3 min | $6\mathrm{cm}$ |
| 4091833 | 81472 | 9.7 | $4.5 \times 1.8 \times 12$ | 1314 | 36.4 min | 8 cm |

Table 4.4: Characteristics and Performance of 3D simulations for different tape lengths

To check these length dependencies we will compare the performance and the field profile of three different tapes of 3 cm, 5 cm and 7 cm. The results are presented in Table 4.4.

We observe that although the remarkable edges' increase the total elapsed time is not affected dramatically. This is thanks to the parallelization in Alya so, by recruiting more the cores the performance is hardly affected.

We should note that even the elapsed time is similar, the queueing of more resources takes more waiting time before the simulation starts. So, although it takes similar times the actual time for larger domains is longer. But we still have to check the magnetic field profile for the three lengths to see if all the cases give results similar to the experimental data.

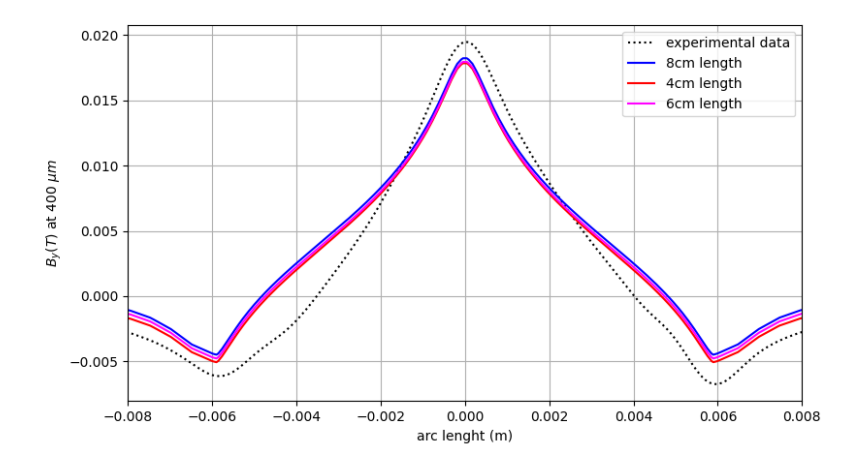


Figure 4.15: Comparison of B_y at $400\mu m$ for different lengths of tapes and experimental values

From figure 4.15 we can deduce that the length of the tape is not affecting much at the final results, the border effect is not present anymore in the 4cm tape. Thus from now on, we will use the 4cm tape. This setup is accurate enough and keeps a low number of resources used. With this, we should be able to add the angular dependence or increase the mesh definition if needed. Also, we know that, eventually, we can increase the length of the tape to get a bit better results but knowing this will be a more demanding simulation.

Another advantage of the 3D simulations is the possibility to reproduce completely the current distribution. In the 2D case, the current loops could be interpreted while assuming that if some current was pointing outwards and some current pointing inwards it had to come from a loop distribution. Besides that, in this case we can visualise the whole loop and check the expected behaviour of the superconductor (see Figure 4.16). Moreover, some

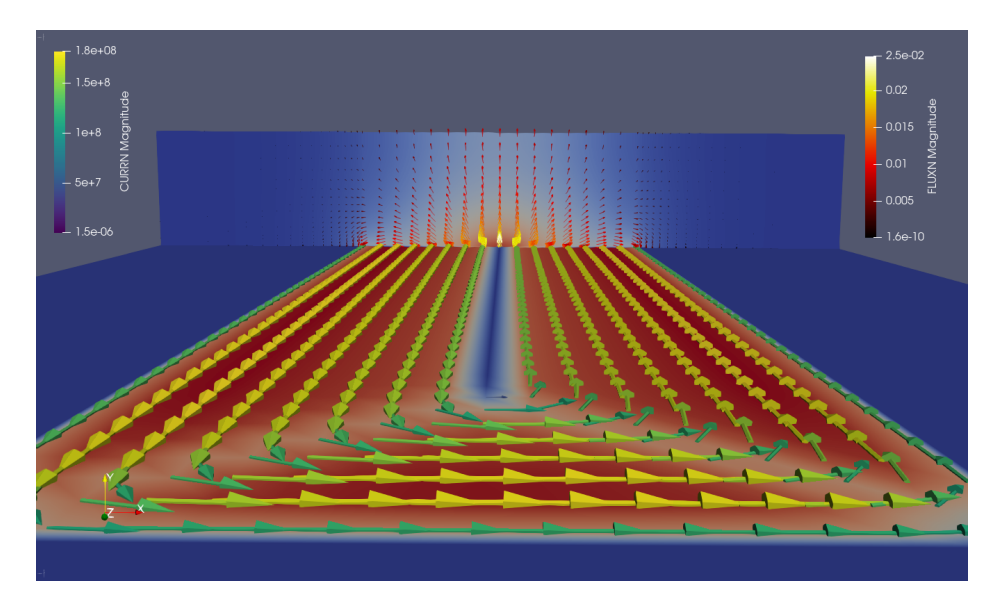


Figure 4.16: 3D plot of the superconducting tape, the vectors show the current flowing in the tape

new phenomena can be seen such as the current distribution on the borders. This behaves equally in the central part of the tape but doing a sudden turn on the diagonal weakening the current in that area.

In addition, any slice done with a normal vector pointing to the z-direction has to look very similar to the 2D simulations and at least the slices done in these *Paraview* simulations look like in the 2D experiments.

4.3.2 3D case with variable Critical Current

Similarly to the 2D case, we will include now the dependent Critical Current. The script used in the 2D for the $J_c(\theta, \mathbf{H})$ will work because the tilted axis is still on the x-y plane so it remains equal than in the 2D simulation. In this case, similarly to the 2D simulations, we find that this dependence complicates the convergence of the problem. That is why we needed to refine the mesh. Moreover, we decreased the minimum time step (dtmin) and increased the tolerance of the solver. With these new updates we could run the simulation and got the following summary:

| Edges | Boundaries | Total space | Cores | Elapsed time |
|---------|------------|-------------------------|-------|--------------|
| 1972322 | 49072 | $6.48 \times 10^{-5} m$ | 584 | 4:43h |

Table 4.5: Summary of the 3D case with $J_c(\theta, \mathbf{B})$

The simulation took more time because of the reduction of dtmin and the convergence problems of the solver. The Preconditioner of the solver will need to be upgraded. For the moment we approximate the inverse of the matrix for the inverse of a diagonal matrix whose diagonal elements are identical to the original diagonal elements of the matrix. This preconditioner is quite basic and does not improve enough the convergence when

the simulation gets more complex. This issue will be commented in the Further Work subsection 5.2.2.

Nevertheless, we got satisfactory results with a better definition than before. In figure 4.17 we have a sketch of the superconducting tape with its currents and magnetic field in the center slice.

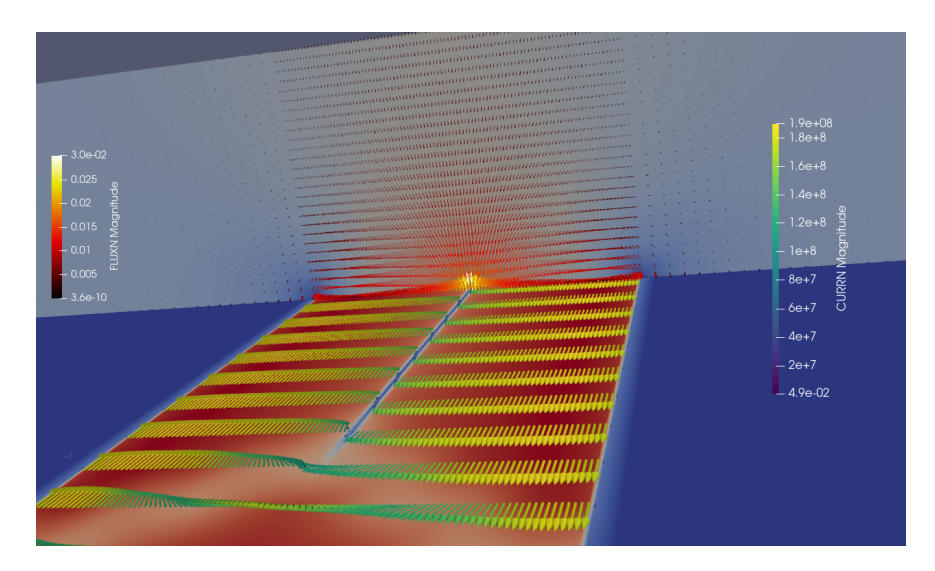


Figure 4.17: Current and Magnetic field of the new 3D simulation

In this plot the phenomenon of the current in the borders can be seen well. Despite this and the highest definition of points, there is no substantial change compared to the older figure 4.16. This suggests that neither in the 2D or the 3D case the $J_c(\mathbf{B}, \theta)$ will be able to represent the asymmetry in the experimental data. By plotting the magnetic field at 400 μm for this case and comparing it to the experimental data we observe a similar result to other simulations.

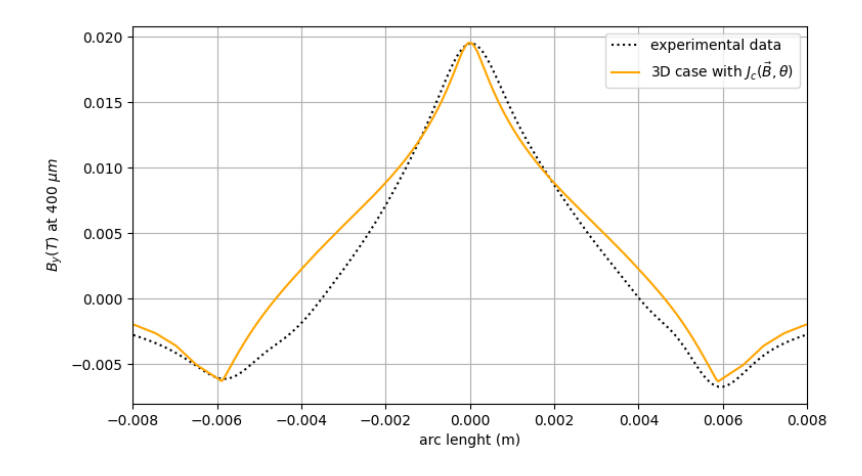


Figure 4.18: B_y at $400\mu m$ for the 3D case with $J_c(\theta, \mathbf{B})$.

4.4 Final Summary and Comparison

Up to now a qualitative comparison has been done, and despite the fact that the results of most simulations have very good agreement with the experimental data, we will go for a more quantitative comparison in order to check which simulation setup gets closer to the experimental data.

The difference between all the plots (see figure 4.19) is very small so we will need for further analysis to determine which one is better.

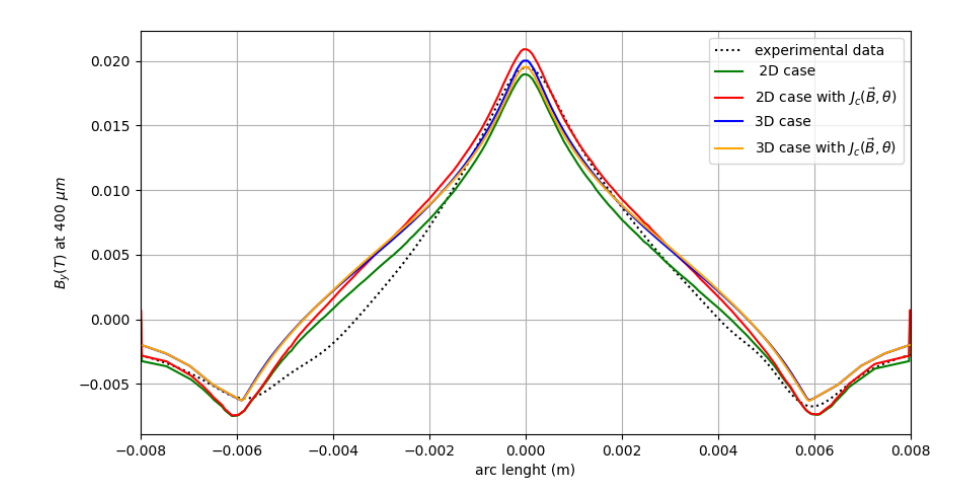


Figure 4.19: Final comparison for Magnetic Field profiles

The strategy now will be to use the magnetic field at 400 μm plots of all the simulations done and calculate for every case the maximum difference (max) and an analogous error version of the Root Mean Squared Deviation used to calculate differences between two vectors (RMSD). As seen in equation 4.4.1, B_s are the simulated values, B_{exp} the experimental values and N the total dimension of the vector.

$$RMSD = \sum_{i=1}^{N} \frac{\sqrt{(B_s^i(x) - B_{exp}^i)^2}}{N}$$
 (4.4.1)

This will lead to a more quantitative analysis.

| | | 2D case | 2D with $J_c(\boldsymbol{B}, \theta)$ | 3D case | 3D with $J_c(\boldsymbol{B}, \theta)$ |
|-----|----------------|---------------|---------------------------------------|---------------|---------------------------------------|
| RM | SD | 2.7431185e-06 | 2.7431187e-06 | 7.6835778e-07 | 7.7155810e-07 |
| max | \overline{c} | 0.00278 | 0.00286 | 0.00405 | 0.00410 |

Table 4.6: Differences between simulations and experimental data

In table 4.6 the results show that the Root Mean Squared Deviation is similar for all the simulations, but the one with the lowest are the 3D case, concretely the one without $J_c(\mathbf{B}, \theta)$. This case has a $RMSD = 7.68 \times 10^{-7}$, closely to this result there is the 3D case

with $J_c(\mathbf{B}, \theta)$ that has just 3×10^{-9} more than the 3D case, and finally we have the 2D cases that have an RMSD between 3-4 times higher than the 3D cases.

We could state that the RMSD of all the simulations can be considered very low. However, the 3D simulations show between 3-4 times less accumulated error than the previous 2D cases. Otherwise, the results are different for the maximum difference. The simulation reaching the lowest maximum difference is the 2D basic case with a maximum difference between values on the same point of 0.00278 T followed just by the 2D case with $J_c(\mathbf{B}, \theta)$ with a total error of 0.00286. Unlike the previous case now the 3D simulations show an increase of more than a 30% concerning the 2D case.

In conclusion, and considering the plots with the error measurements, the results from all simulations have a good agreement with the experimental data. The 3D cases show an improvement with respect to the 2D cases when we measure the accumulated error, decreasing the error by a factor of almost 4. On the other hand, the 2D cases show less point-to-point maximum deviation from the experimental values with a maximum difference of 30% less than the 3D cases.

In general, the 3D simulations lead to slightly better results as a main behavior but with some points with less accuracy than in the 2D cases. Furthermore, the 3D simulations allow to observe phenomena that cannot be seen with the 2D simulations, such as the current loops and the border effects. The most relevant drawback of these simulations is the computational cost. For the 2D simulations, 80 cores were enough to run the case but for the 3D we needed between 7 to 15 times more computational resources with a maximum case of 1300 cores for the 8 cm long tape.

So, to obtain preliminary results the 2D case could be enough but for more accurate and decisive studies, and also to be able to include all the physical phenomena, the 3D case is needed. To perform further studies of this kind, a supercomputer and a dedicated HPC code such as Alya are strictly required.

Chapter 5

Conclusions

The main results of the thesis will be summarised in this chapter with an outlook on the applicability of this work and the prospects for future research and development.

5.1 Summary

The main goal of this thesis was to do a first validation of the magnet module of the HPC finite element code Alya for superconductivity experiments. This is a first step on the development of a multiphysics code for simulating HTS and its consequent applications in the fusion domain. Also, some new implementations and modifications have been added to the code to make it more adaptable to real cases, for example the variable critical current in terms of the Magnetic Flux and the direction of the field.

Previous to the validation of the code, good understanding of superconductivity was required, including their classifications, and the different numerical approaches when simulating them. We went through different formulations of Maxwell equations and saw how the \boldsymbol{H} formulation is a suitable model to simulate the macroscopic behavior of superconductors. Moreover, we have got familiarised with a supercomputer environment and an HPC code Alya. We researched the structure and operation of Alya and its module magnet.

A summary of Finite Elements has been done to understand better the numerical techniques used by Alya to solve these problems. Finally, first detailed explanation about the magnet module has been done, with its working procedure, and a deep explanation of all the input and necessary files for running a simulation.

The main goal mentioned in chapter 1 has been achieved by all the simulation setups leading to good agreement between the simulations and the experimental data. It could be checked how some setups represent better the experimental data than others, but in general, all the consistent setups gave close values to the ICMAB data as well as physical coherent phenomena. Hence we can conclude they gave a good representation of the superconducting tape.

In particular, the 2D results have shown very good agreement when reproducing the field at 400 μm . Concretely the case of the 2D mesh without the self field and a large air

domain including $J_c(\mathbf{B}, \theta)$ has shown to be the best compared to the experimental data among the 2D cases simulated. But all the other cases in 2D remain close to this setup. The only drawback was the impossibility to reproduce an asymmetry in the y component of the magnetic field.

The only case which was leading to a non converging simulation was the combination of deactivating the Self-Field and a small domain. This convergence problems are attributed to the lack of air and the Biot-Savart implementation. In conclusion, we could extract that all combinations need to have either a big air domain or the Self Field option active. On the other hand, the Self Field option leads to minor convergence problems when the field tends to zero. To avoid problems a good setup is big air domains with Self Field deactivated.

The implementation of $J_c(\mathbf{B}, \theta)$ has been done successfully affecting the current distribution on the tape. However the tilting of the tape structures and using a variable Critical Current density could not reproduce the asymmetries observed in the experimental data. Another drawback is the fact that Alya took more time to solve these simulations. This caused minor convergence problems when this dependence was included so the tolerance and dtmin of the solver had to be changed to achieve good results.

For the 3D cases, a good agreement has also been found between the simulations and the experimental data but also caused a big increase in the resources needed.

However, the elapsed time was hardly affected when increasing the tape length and proportionally the number of nodal points on the mesh. That is given by the efficient parallelization done by Alya and reaffirms its suitability for HPC.

A brief study has been done to optimize the length of the tape in the simulations. The conclusion obtained is that even though the experimental tape is 12 cm long, the length of the simulated tape does not affect the magnetic field profile. A simulated tape of 4 cm was still giving good results reducing the elements of the mesh by 3.

The 3D simulations, despite giving very similar results as the 2D case, allowed us to see some physical phenomena in the tape such as the current loops created in a Superconductor or the current effects in the borders. This could not be seen in the 2D simulations although the main features can be derived from the 2D results.

In the final quantitative comparison, the 3D simulations have shown better results getting a smaller RMSD, concretely the 3D case with variable Current Density reached an improvement of 4 times less error compared to the experimental results than the 2D cases. Besides that, the 2D cases have shown to have less local deviation because the maximum difference point-to-point in the 2D cases is a 30% smaller than the 3D cases. This means that globally the 3D cases have better accuracy but in some concrete points keep more error than the 2D cases.

One general conclusion is that with Self-Field off and including a large air domain while activating J_c , all simulations set-ups lead to good simulation results.

2D simulations needed an acceptable amount of resources but especially the 3D simulations can only be done efficiently and with a realistic elapsed time by using a supercomputer like *Marenostrum* 4 and a dedicated HPC code Alya. Otherwise, the management of a problem composed of 1.3M nodes for thousands of time steps could lead to parallelization problems

coming from the communication between nodes. Alya was able to run this simulation with 1300 cores in only 30 minutes. However, the simulations take longer when implementing the variable Critical Current, this can be due to the not good enough preconditioner of the algebraic solver.

5.2 Outlook and Future Work

This thesis has successfully completed the first steps in the validation of the module magnet in Alya for simulating Superconductivity. Despite this, there is a long road ahead. There are two main topics where further work can be done. The magnet module still has some parts where it can be improved and this will be discussed below. On the other hand, some more work can be developed on Superconductivity modelling apart from improving the module itself, this will be discussed in the latest section.

5.2.1 Improving magnet module

The magnet module has been developed using the H-Formulation and Finite Element Methods and this shows to work well with the Superconductivity experiment. But there is an approximation used in these simulations set up that stays far from realistic. The resistivity of the air is set to be in the range of $10^{-2} - 10^{-4} \Omega$, which is far from the real value of air resistivity $(1.3 \times 10^{16}\Omega)$. This together with the convergence problems encountered in some particular situations might be possible to solve in the following different ways that still need to be explored and could be implemented in this module:

- **Preconditioner Improvement**: The preconditioner used in the Algebraic Solver is one of the most basic preconditioners when solving a system of equations. The assumption is that the solution will be similar to the diagonal of the linear system. It helps very often but sometimes leads to convergence problems.
 - Further work is being carried out in the BSC Fusion Group to develop an improved preconditioner which approximates the solution better than the actual one. This could suppose a big improvement on the convergence of complicated meshes or situations, which now require very small time steps or more drastic changes such as new meshes. It could even help to increase the resistivity of the air to a more realistic value.
- Different Formulations for each Domain: For the moment, the *H*-Formulation has been used in the module because it is the most suitable for calculating variable magnetic fields. This formulation seems to be working very well in conductor or superconductor materials. However for vacuum, air, or other resistive domains other formulations could be more appropriate. For example, the *A*-Formulation looks promising for this kind of domain because you can input the current as a boundary condition and so there would not be problems regarding the resistivity of the air.

This would mean to couple different formulations for different domains and in some parts of the input files like the simulation.mag.dat you could specify which formulation you want to solve for each problem.

The A-Formulation does not seem to be difficult to implement because of its similarities with the H-Formulation. The complicated part would be to couple the formulations and have an agreement on the boundaries.

• Shell elements: Shell elements is a technique used mainly in solid mechanics simulations. It consists on substitute the air around the tape by boundaries of the domain of interest which are non-spatial boundaries but 2-dimensional (in the 3d cases). This improvement can be one of the most difficult to implement and there is not any precedent using this technique. However it can reduce substantially the number of elements of the simulation as well as the air problem. Hence despite the drawbacks it looks like a promising option.

5.2.2 Further Work regarding Superconductivity

Apart from improving the module itself, there are some possibilities to follow to do relevant simulations about superconductivity.

As a short-term further work, we are currently simulating experiments on AC losses. Now that the module has been validated for simple experiments we can go for more complex simulations such as the measurement of the energy losses when applying an external AC field. The dependence of the energy loss with the frequency shows how these losses change when switching the geometry or using stacks of tapes instead of single tapes.

Moreover, as explained in subsection 2.4.1 the phenomena of Quench are very relevant in the world of superconductivity applications. It is very costly to study if it is not done with simulations. The variation in temperature affects directly the Critical Current of the superconductor (even bringing it out of the superconductor state) and the resistive state affects back the temperature of the material.

For simulating quench the module of magnet is not enough, the coupling between the magnet module and a further existing Alya module temper for heat transfer is required. Hence a simulation can be checking at every timestep the two physics and send information between them. Because of the strongly dependent physics, some relations between the modules need to be investigated and checked apart from just coupling the two modules. In a summary, the HTS multiphysics capabilities are necessary to simulate Quench, and in consequence, the development of the HTS modelling.

There are still a lot of topics of interest regarding superconductivity and an HPC code like Alya in a supercomputer and a dedicated module like magnet can be very helpful to design and optimize superconductor HTS devices (such as cables and machinery). These lines would be crucial to develop new tools to analyze three-dimensional complex geometries to optimize engineer's designs. Furthermore, the emerging analysis themselves would be new interesting cases that can be valuable for the scientific community.

Bibliography

- N. Amemiya, S.-I. Murasawa, N. Banno, and K. Miyamoto. Numerical modelings of superconducting wires for ac loss calculations. *Physica C: Superconductivity*, 310(1): 16–29, 1998. ISSN 0921-4534. doi: https://doi.org/10.1016/S0921-4534(98)00427-4. URL https://www.sciencedirect.com/science/article/pii/S0921453498004274.
- Z. Bofang. Front Matter, pages i-xxvi. John Wiley & Sons, Ltd, 2018. ISBN 9781119107323. doi: https://doi.org/10.1002/9781119107323.fmatter. URL https://onlinelibrary.wiley.com/doi/abs/10.1002/9781119107323.fmatter.
- CASE department. Alya's system user's documentation., 2021. URL https://gitlab.com/bsc-alya/alya/-/wikis/home.
- D. V. Delft. History and significance of the discovery of superconductivity by Kamerlingh Onnes in 1911. *Physica C: Superconductivity and its applications*, 479:30 35, 2012. ISSN 0921-4534. URL https://login.are.uab.cat/login?url=http://search.ebscohost.com/login.aspx?direct=true&db=edselp&AN=S0921453412000962&site=eds-live.
- P. Drude. Zur Elektronentheorie der Metalle. Annalen der Physik, 306(3):566-613, 1900. doi: https://doi.org/10.1002/andp.19003060312. URL https://onlinelibrary.wiley.com/doi/abs/10.1002/andp.19003060312.
- J. Dular, C. Geuzaine, and B. Vanderheyden. Finite-element formulations for systems with high-temperature superconductors. *IEEE Transactions on Applied Superconductivity*, 30 (3):1–13, 2020. doi: 10.1109/TASC.2019.2935429.
- F. Grilli. Numerical modeling of hts applications. *IEEE Transactions on Applied Superconductivity*, 26:1–1, 04 2016. doi: 10.1109/TASC.2016.2520083.
- Z. Hong, A. M. Campbell, and T. A. Coombs. Numerical solution of critical state in superconductivity by finite element software. Superconductor Science and Technology, 19 (12):1246–1252, oct 2006. doi: 10.1088/0953-2048/19/12/004. URL https://doi.org/10.1088/0953-2048/19/12/004.
- X. Huang, X. Wang, D. Duan, B. Sundqvist, X. Li, Y. Huang, H. Yu, F. Li, Q. Zhou, B. Liu, and T. Cui. High-temperature superconductivity in sulfur hydride evidenced by alternating-current magnetic susceptibility. *National Science Review*, 6(4):713–718, 05 2019. ISSN 2095-5138. doi: 10.1093/nsr/nwz061. URL https://doi.org/10.1093/nsr/nwz061.
- ITER project. ITER documentation., 24 October, 2007. URL https://www.iter.org/proj/inafewlines.

- G. Karypis. Metis documentation., accessed: February 9, 2022. URL https://glaros.dtc.umn.edu/gkhome/metis/metis/overview.
- D. Kuzmin and J. Hämäläinen. Finite Element Methods for Computational Fluid Dynamics: A Practical Guide. Society for Industrial and Applied Mathematics, Philadelphia, PA, 2014. doi: 10.1137/1.9781611973617. URL https://epubs.siam.org/doi/abs/10.1137/1.9781611973617.
- F. London and H. London. The electromagnetic equations of the supraconductor. *Proceedings of the Royal Society of London. Series A Mathematical and Physical Sciences*, 149 (866):71–88, Mar. 1935. ISSN 1471-2946. doi: 10.1098/rspa.1935.0048. URL http://dx.doi.org/10.1098/rspa.1935.0048.
- J. Lorenzo. Private Communication, Barcelona Supercomputing Center, 2019.
- F. López and J. Costa. *Interacción electromagnetica, teoria clásica*. Editorial Reverté, 2000. ISBN 9788429130584.
- J. C. Maxwell. Viii. a dynamical theory of the electromagnetic field. *Philosophical Transactions of the Royal Society of London*, 155:459–512, 1865. doi: 10.1098/rstl.1865.0008. URL https://royalsocietypublishing.org/doi/abs/10.1098/rstl.1865.0008.
- MUMPs. MUltifrontal Massively Parallel sparse direct Solver documentation., accessed: February 9, 2022. URL http://mumps.enseeiht.fr/.
- R. Pecher, M. Mcculloch, S. Chapman, L. Prigozhin, and C. M. Elliott. 3D-modelling of bulk Type-II Superconductors using unconstrained H-formulation. *Proc. 6th EUCAS, Sorrento*, Italy, 2003, 2003.
- PJRay, Wikipedia. Overview of superconducting critical temperature., 19 November 2015. URL https://commons.wikimedia.org/wiki/File:Timeline_of_Superconductivity_from_1900_to_2015.svg.
- Y. Saad. *Iterative Methods for Sparse Linear Systems*. Society for Industrial and Applied Mathematics, second edition, 2003. doi: 10.1137/1.9780898718003. URL https://epubs.siam.org/doi/abs/10.1137/1.9780898718003.
- simscale.com. Boundary conditions review., accessed: February 9, 2022. URL https://www.simscale.com/docs/simwiki/numerics-background/what-are-boundary-conditions/.
- M. Solazzo, F. O'Brien, V. Nicolosi, and M. Monaghan. The rationale and emergence of electroconductive biomaterial scaffolds in cardiac tissue engineering. *APL Bioengineering*, 3:041501, 12 2019. doi: 10.1063/1.5116579.
- Y. Strelniker, A. Frydman, and S. Havlin. Percolation model for the superconductor—insulator transition in granular films. *Physical Review B*, 76, 01 2007. doi: 10.1103/PhysRevB.76. 224528.
- THEVA. Scheme of the THEVA tape., accessed: February 9, 2022. URL https://www.theva.com/products/.

E. Vinot, G. Meunier, and P. Tixador. Different formulations to model superconductors. $IEEE\ Transactions\ on\ Magnetics,\ 36(4):1226-1229,\ 2000.\ doi:\ 10.1109/20.877661.$

Appendix A

Setting up the boundary conditions and the critical current dependencies in the magnet module

Apart from the input files of the module described in 3, there are other important files and scripts relevant for the set up of the simulation. As discussed in subsection 3.4.2 there are mainly two files to take in account, i.e. MOD_MAG_INPDAT.f90 for the boundary conditions and initial conditions and MOD_MAG_MATPRO.f90 for the dependencies of the Critical Current.

The summary below of these files will be done only for the code parts relevant for this thesis. The code on each file is substantially longer, with more inputs and cases but they are not necessary for this work.

A.1 Boundary Conditions

The file responsible for the Boundary Conditions is MOD_MAG_INPDAT.f90. In this file out of the whole script we can find two main parts in which we are interested in, the initial conditions and the contour conditions. The initial condition is such that:

The function mag_inifie(x) defines the magnetic field \mathbf{H} in all the domain at the beginning, in this case we observe how it is set to be zero except for the second component of the field which is $0.5/\mu_0$, which is the initial condition stated in subsection 3.4.2.

```
function mag_dirfie(t, x) result(field)
     if (size(x) = 2 - ip) then
       ! TAPE2D EXTERNAL FIELD
       if (t \le 0.005 \text{ rp}) then
         field = 0.5 rp / mu0_mag * cos(100.0 rp * pi * t) * [0.0 rp, 1.0 rp]
         field = [0.0 \text{ rp}, 0.0 \text{ rp}]
       !ଉର୍ଗ୍ରେସ୍ପର୍ପ୍ରସ୍ତ୍ରପ୍ରସ୍ତ୍ରପ୍ରସ୍ତ୍ରପ୍ରସ୍ତ୍ରପ୍ରସ୍ତ୍ରପ୍ରସ୍ତ୍ରପ୍ରସ୍ତ୍ରପ୍ରସ୍ତ୍ରପ୍ରସ୍ତ୍ରପ୍ରସ୍ତ୍ରପ୍ରସ୍ତ୍ରପ୍ରସ୍ତ୍ରପ୍ରସ୍ତ୍ରପ୍ରସ୍ତ୍ରପ୍ରସ୍ତ୍ରପ୍ରସ୍ତ୍ରପ୍ରସ୍ତ୍ରପ୍ରସ୍ତ୍ରପ୍ରସ୍ତ୍ରପ୍ରସ୍ତ୍ରପ୍ରସ୍ତ୍ରପ୍ରସ୍ତ୍ରପ୍ରସ୍ତ୍ରପ୍ରସ୍ତ୍ରପ୍ରସ୍ତ୍ରପ୍ରସ୍ତ୍ରପ୍ରସ୍ତ୍ରପ୍ରସ୍ତ୍ରପ୍ରସ୍ତ୍ରପ୍ରସ୍ତ୍ରପ୍ରସ୍ତ୍ରପ୍ରସ୍ତ୍ରପ୍ରସ୍ତ୍ରପ୍ରସ୍ତ୍ରପ୍ରସ୍ତ୍ରପ୍ରସ୍ତ୍ରପ୍ରସ୍ତ୍ରପ୍ରସ୍ତ୍ରପ୍ରସ୍ତ୍ରପ୍ରସ୍ତ୍ରପ୍ରସ୍ତ୍ରପ୍ରସ୍ତ୍ରପ୍ରସ୍ତ୍ରପ୍ରସ୍ତ୍ରପ୍ରସ୍ତ୍ରପ୍ରସ୍ତ୍ରପ୍ରସ୍ତ୍ରପ୍ରସ୍ତ୍ରପ୍ରସ୍ତ୍ରପ୍ରସ୍ତ୍ରପ୍ରସ୍ତ୍ରପ୍ରସ୍ତ୍ରପ୍ରସ୍ତ୍ରପ୍ରସ୍ତ୍ରପ୍ରସ୍ତ୍ରପ୍ରସ୍ତ୍ରପ୍ରସ୍ତ୍ରପ୍ରସ୍ତ୍ରପ୍ରସ୍ତ୍ରପ୍ରସ୍ତ୍ରପ୍ରସ୍ତ୍ରପ୍ରସ୍ତ୍ରପ୍ରସ୍ତ୍ରପ୍ରସ୍ତ୍ରପ୍ରସ୍ତ୍ରପ୍ରସ୍ତ୍ରପ୍ରସ୍ତ୍ରପ୍ରସ୍ତ୍ରପ୍ରସ୍ତ୍ରପ୍ରସ୍ତ୍ରପ୍ରସ୍ତ୍ରପ୍ରସ୍ତ୍ରପ୍ରସ୍ତ୍ରପ୍ରସ୍ତ୍ରପ୍ରସ୍ତ୍ରପ୍ରସ୍ତ୍ରପ୍ରସ୍ତ୍ରପ୍ରସ୍ତ୍ରପ୍ରସ୍ତ୍ରପ୍ରସ୍ତ୍ରପ୍ରସ୍ତ୍ରପ୍ରସ୍ତ
        ! BENCH3D
        if (t \le 0.005 \text{ rp}) then
                      field = [0.0 \text{ rp}, 0.5 \text{ rp}, 0.0 \text{ rp}] * 1.0 \text{ rp} / mu0 \text{ mag} * cos
    (100.0 \text{ rp} * \text{pi} * \text{t})
        else
                      field = [0.0 rp, 0.0 rp, 0.0 rp]
          end if
   end if
```

Here we have a similar function called mag_dirfie(t,x). This case depends on the time, there is a differentiation for 2D or 3D with this if(size(x) == 2_ip), in this case it means the size of the vector is 2 and so it is 2D, for the else option we have the 3D case.

Here the condition of the external field is set, for time lower than $0.005\ s$ the field follows the cosine function but afterwards is just set to zero. The same happens for the 3D case with the difference that 3 components need to be declared.

A.2 Dependencies on the Critical Current

The file MOD_MAG_MATPRO.f90 is responsible for the Critical Current dependencies. When in the input file simulation.mag.dat the critical current J_c is set as USERD, Alya will take the value of J_c from this file.

```
Jc = (189.53456_rp/0.0000012_rp) * (1+((sqrt(dot_product(Hmag,Hmag))*mu0_mag
   )/(0.05184 \text{ _rp}))**(-0.50016 \text{ _rp}) * (1-((sqrt (dot \text{_product} (Hmag, Hmag)))*
   mu0\_mag)/(7.22788\_rp)))**2.0\_rp
       if(Hmag(2) == 0) then
          if (Hmag(1) < 0)then
             theta = (3 * 3.141592 \text{ rp})/2
             theta = 3.141592 \, \text{rp} / 2
          end if
      else
         theta = atan(Hmag(1)/Hmag(2))
         if(Hmag(1)>0)then
                  if(Hmag(2)>0)then
                       theta = theta
                   else if (Hmag(2) < 0)then
                       theta = 3.141592_rp + theta
                  end if
         else if (Hmag(1) < 0)then
                  if (Hmag(2) < 0) then
                        theta = 3.141592 rp + theta
                  else if (Hmag(2) > 0)then
                         theta = 2*3.141592_rp+theta
                  end if
         end if
      end if
     if (theta > 3.141592 rp) then
        theta=theta-3.141592_rp
     end if
!change from radians to degree due to the interpolation
      degree = theta * 360.0 _{rp} / (2 * 3.141592 _{rp})
      Jc = Jc *(1/interpLinear1(intp1_mag(1),30.00_rp)) * interpLinear1(
   intp1_mag(1), degree
     ! Jc = Jc *(1/0.209325983148271 \text{ rp}) * interpLinear1(intp1_mag(1), theta)
 !interpLinear1(intp1_{-}mag(1), 0.2_{-}rp)
    case (-1_ip)
      Jc = 0.0 \text{ rp}
    case default
      Jc = 0.0 \text{ rp}
      call runend ('mag_scalin: unknown scaling law')
    end select
end function mag_scalin
```

First, out of all the cases in the if loop, the one used for J_c is the case 9. Hence if any change needs to be done, it has to be in this if loop.

Apart from this, the first part is the equivalent of the equation 4.2.4. After this a angle change is done because the angle given is from $0 - \pi/2$ and the parametrisation is done from $0 - 2\pi$, hence looking the quadrant of each vector we can find the real angle of each vector. Afterwards there is a change to degrees because the lift factor parametrized is given in

degrees, and the interpolation of the lift factor is done with the interpLinear1() function. Finally the whole computation of J_c is done using the expression 4.2.5.